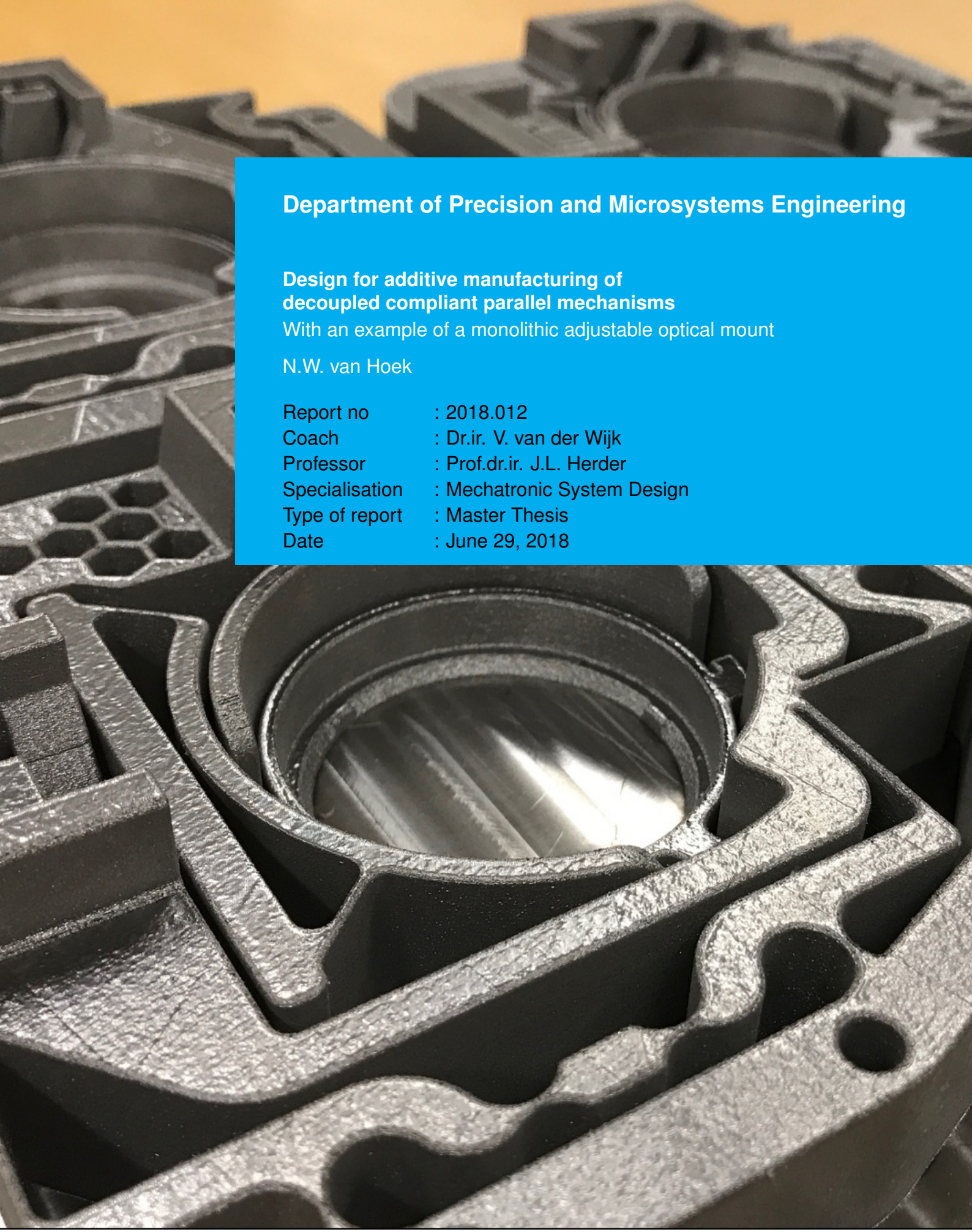

Department of Precision and Microsystems Engineering

Design for additive manufacturing of decoupled compliant parallel mechanisms

With an example of a monolithic adjustable optical mount

N.W. van Hoek

Report no	: 2018.012
Coach	: Dr.ir. V. van der Wijk
Professor	: Prof.dr.ir. J.L. Herder
Specialisation	: Mechatronic System Design
Type of report	: Master Thesis
Date	: June 29, 2018

TU Delft Delft University of Technology

Challenge the future

Design for additive manufacturing of decoupled compliant parallel mechanisms

With an example of a monolithic adjustable optical mount

by

N.W. van Hoek

to obtain the degree of Master of Science
at the Delft University of Technology,
to be defended publicly on Friday June 29 at 12.00 PM

Student number:	4245105	
Project duration:	September 5, 2016 – June 29, 2018	
Thesis committee:	Prof. dr. ir. J. L. Herder,	TU Delft, supervisor
	Dr. ir. V. van der Wijk,	TU Delft, daily supervisor
	Dr. ir. M. Langelaar,	TU Delft
	Dr. ir. G. Oosterhuis,	VDL Enabling Technologies Group

An electronic version of this thesis is available at `http://repository.tudelft.nl/`.

TU Delft

VDL Enabling Technologies Group

Preface

This thesis is the conclusion the Precision and Micro-systems Engineering Master's programme at Delft University of Technology. I have had the pleasure of fulfilling this program in the fun and inspiring work environment of the department of Precision and Micro-systems Engineering and feel honoured to have contributed to this environment as board member of study association Taylor. On top of this I have had the amazing opportunity to carry out this research at the VDL ETG office in Milpitas, California. Which has been an educational experience on both a professional and personal level.

This research is sponsored and hosted by VDL Enabling Technolgies Group. The main results are provided in a paper which is preceded by a literature investigation.

This project would not have been completed without the support and guidance of a number of people. First of all, I would like to thank my daily supervisor Volkert van der Wijk for his guidance, even when I was across the globe. His flexibility and our meetings significantly increased the pace of my progress and his thorough feedback taught me a lot about academic writing. I would also like to thank Just Herder, for helping me find this project, connecting me to VDL ETG and our educational regular meeting during the first phase of this project.

I would like to give special acknowledgement to my supervisor at VDL ETG, Gerrit Oosterhuis. Without his guidance on both the technical and organizational aspects of the project I would not have come close to manufacturing a prototype. He outdid his job as supervisor by helping me out on personal and logistic issues associated with moving to the USA. I would also like to thank the rest of the VDL ETG USA west-coast team: Peter Severeijns, Rob van Wouw, Wilfried van Kessel, Gerjan Veldhuis, Frank Hochstenbach, Patrick Dijk, Raymond Chan, Patrick Dijk and Aik Beng Ong. Who made me feel welcome as soon as I walked in and supported me on a both professional and personal basis.

I want to give special recognition to my fellow Taylor board members: Thijs, Miranda, Maarten and Menno. Who often offered some desired distraction. I am also grateful for my fellow graduate students in my office with whom I could often discuss and complain about my progress.

I am thankful for my friends who have been supporting even in times when they did not see me for weeks.

Finally, I am most thankful for the relentless support of my amazing parents, Caspar and Astrid, and my sisters, Anne and Wies. None of this would have been possible without their full support.

Niek van Hoek
Delft, June 2018

Contents

1 Introduction

Compliant mechanisms are, like rigid-body mechanisms, used to transfer or transform motion, force or energy [19]. However, rigid-body mechanisms are comprised of ridged parts which can move with respect to each other by means of revolute and sliding joints. The motion of compliant mechanisms comes from deflection of flexible parts [20]. Compliant mechanisms have several advantages over rigid-body mechanisms which makes them practical in a variety of applications such as: medical instruments, micro-manipulators and micro-electro-mechanical systems [5, 22, 23]. In these applications the compliant mechanisms have advantages in performance due to increased precision and reliability, and reduced wear, weight and reduced maintenance. They could also result in cost reduction because they require less parts, the assembly time is reduced and the manufacturing processes are simplified [19].

However, designing compliant mechanisms also comes with several challenges. They require simultaneous design for motion and force behaviours and the range of motion is limited [20]. Accurate knowledge of the force-displacement characteristics for different geometries is required. Furthermore, the stiffness in the direction of the degrees of freedom (DOFs) is not equal to zero and the stiffness in the constraint direction is limited [35]. As a result of undesired compliance the compliant mechanisms often suffer from cross-axis coupling between DOFs and parasitic motion in constrained directions. These undesired motions could significantly reduce the precision of an mechanism. Since compliant mechanisms are often used in applications where micro, or even nano meter precision is required it is important to prevent this behaviour. Smart designs are required to decouple the DOFs and reduce crosstalk between DOFs [26].

Compliant mechanisms can be manufactured using various methods. Common methods are wire electric discharge machining, milling or casting [18]. These methods may have limited design freedom, become more expensive with the complexity of the design or are expensive for production of a few products. Advancements in additive manufacturing (AM) result in increasing quality of products and more choice in materials. The additive manufacturing processes build the product by stacking thin layers of material on top of each other. Using this method, a wide variety of geometries, simple and complex, can be produced at relatively low costs. Adjustments in the design do not require modifications of the production production line. However, the resolution of features is limited by the thickness of the layers and the width of the melt pool or extrusion diameter. Also, some geometries require support structures to support floating or overhanging features during the AM process. These structures need to be removed afterwards at the cost of more post-processing steps [8, 42].

This thesis provides a design approach for additive manufacturing of decoupled parallel compliant mechanisms to provide a guideline for designers to exploit the advantages of additive manufacturing while reducing costs and improving the final quality of the product. This is done by first investigating literature on the design of decoupled compliant mechanisms to find approaches to decouple mechanisms and reduce cross-axis coupling and parasitic motion. Previous research has been categorized by the DOFs of the mechanism. For each category the used kinematic architectures are summarized and some approaches to reduce cross-axis coupling and parasitic motion are given. The results of this investigation can be found in chapter 2. In chapter 3, the main chapter, a design approach is proposed for additive manufacturing of compliant mechanisms. Together with the outcomes of chapter 2 a design is made for a four DOF decoupled monolithic compliant alignment mechanism. This design is manufactured and experimentally evaluated to validate the viability of additive manufacturing for the production of high-precision compliant mechanisms. The results from this research are discussed in chapter 4 followed by a conclusion in chapter 5.

2

Investigation of decoupled compliant parallel mechanisms

2.1. Introduction

Compliant mechanisms are used in applications where high-precision is demanded, such as: microchip assembly, cell manipulation, atomic force microscopy and optical alignment [39]. Compliant mechanisms transfer loads or displacements by deformation a compliant structure. This eliminates backlash, wear and the need for lubrication. The wear and noise of the mechanism is reduced and are simple and inexpensive to manufacture and assemble [15, 35].

A mechanism with multiple degrees of freedom (DOF) is decoupled when each actuator actuates one independent output motion which is not affected by any other actuator. For example, a stage which has to move in X or Y direction has two actuators where actuation of one actuator only results in an output displacement in X direction and the other actuation only results in an output displacement in Y direction. A decoupled mechanism especially improves positioning time when manual actuation is used, since the coupling would mean that an operator has to iteratively adjust the position using multiple actuators which increases positioning time. Manual actuation is often used in optical alignment mechanism where high positioning accuracy is required. The amount of motion in any DOF other than the intended DOF is called cross-axis coupling and the amount of motion in any constraint direction is called parasitic motion [20]. Since the DOFs of a system are actuated the cross-axis coupling can be controlled and the errors can be iteratively reduced until the cross-axis coupling is smaller than the adjustment resolution. Low cross-axis coupling is desired for quick convergence.

Compliant mechanisms have a serial or parallel kinematic structure. Most serial designs have nested 1 DOF stages, which makes them easier to design and gives them decoupled DOFs. Stacking of these stages results in accumulation of position errors and reduced dynamic performance since the moving actuators increase the inertia of the system. Parallel structures on the other hand result in stable mechanisms with a high accuracy and since the actuators can be mounted on the base the dynamic performance increases [29].

A disadvantage of the decoupled compliant parallel mechanisms (DCPMs) is that they tend to be significantly more complex since the motion stage is suspended by multiple kinematic chains which both transfer the actuation motion and isolate the actuators from harmful off-axis forces [27]. By investigating previous research on DCPMs it is aimed to find out how to design a DCPM with reduced cross-axis and parasitic motion errors.

The goal in this chapter is to investigate decoupled compliant parallel mechanisms from literature and compare them for their cross-axis coupling and parasitic motions. The designs from literature will be categorized by their DOFs. For each category the used kinematic structures, flexure modules and compliant elements are evaluated. Followed by the approaches the author used to reduce cross-axis coupling and parasitic motion.

Section 2.2 is divided in subsections for each category. In each subsection the topology en design considerations from literature are evaluated. The observations made in this literature study will be discussed in section 2.3 and conclusions are listed in section 2.4.

2.2. Decoupled compliant mechanism designs

Literature shows a number of compliant parallel mechanisms. Various types can be found: planar mechanisms such as XY and $XY\theta_z$ and spatial mechanisms such as XYZ and 6-DOF. However, most mechanisms with one or more rotational DOFs have a coupling between the output DOFs. Planar $XY\theta_z$ mechanisms as designed by Lu [31] have a coupled output since one actuator does not result in a displacement or rotation in one DOF or have only 1 DOF decoupled from the other DOFs[3]. The same for 6-DOF DCPMs which are based on the steward platform [30, 32, 37] or variations with orthogonal legs [15, 44, 45]. Guo [9] claims this design is fully decoupled since equal actuation of 2 actuators results purely in a translation and opposite actuation results purely in a rotation. In this study solely the decoupled mechanisms were one actuator actuates one DOF are included. For the parallel XY and XYZ mechanisms a variety of decoupled designs can be found which apply various approaches to reduce cross-axis coupling and parasitic motion. The architecture of the parallel mechanisms have a motion stage which is suspended by parallel kinematic chains. These chains are comprised of kinematic joints such as the prismatic (P) and revolute (R) joints. For compliant mechanisms these kinematic joints are replaced by flexure modules which have the same DOFs. These flexure modules get their compliance from compliant elements such as flexure beams. The designs for XY and XYZ DCPMs will be evaluated in this section.

2.2.1. Translational two degree of freedom mechanisms

A significant amount of research has been done on DCPMs with two translational DOFs. The resulting designs are based on a simple 2-PP rigid-body mechanism as shown in figure 2.1. In this mechanisms the motion stage is suspended by 2 legs with two orthogonal prismatic joints in series. The first prismatic joint is actuated and the second joint isolates the actuated joint from the transverse motion of the stage. While some DCPM designs use this 2-PP structure [6, 11], other designs have a 4-PP structure with two actuated legs and two passive legs to have a symmetric mechanism to reduce parasitic-motion [1, 4, 13, 17, 21, 25, 27, 29, 38, 40, 43, 46].

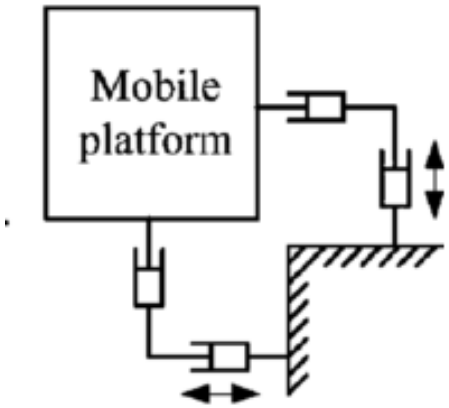

Figure 2.1: Kinematic model of a parallel mechanism with two double prismatic joints[29]

Using this design as starting point a compliant mechanisms can be designed by replacing the prismatic joint with flexure module acting as a linear guiding mechanism. The basic parallelogram flexure module (figure 2.2a) allows linear motion and constrains all other DOFs, which would make it suitable to use as compliant prismatic joint. However, the parallelogram flexure module has a shortening effect where a displacement in the free DOF results in an off-axis error in the direction of the flexures which is equal to [36]:

$$\Delta y = -0.6 \cdot \frac{(\Delta x)^2}{L} \tag{2.1}$$

This shortening effect can be avoided by using a symmetric flexure module where the parallelogram module is mirrored at the axis of translation as shown in figure 2.2b [17]. A double flexure module would compensate the shortening effect by means of an intermediate stage as shown in figures 2.2c and 2.2d. This configuration would also double the range when flexures of the same length are used. However, The under-constraint

secondary stage would reduce the dynamic performance.

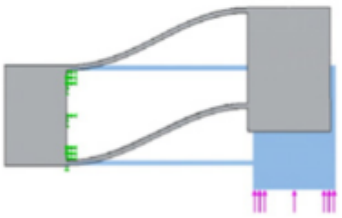

(a) Parallelogram flexure module

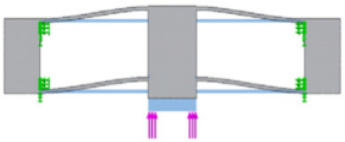

(b) Compound parallelogram flexure module

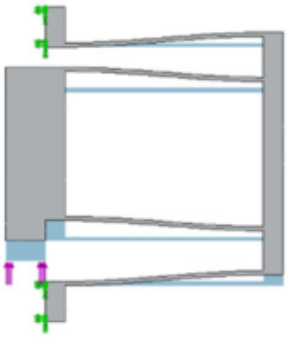

(c) Double parallelogram flexure module

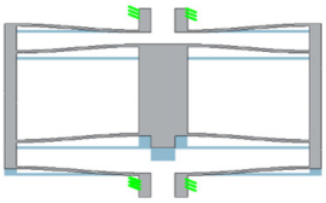

(d) Compound double parallelogram flexure module

Figure 2.2: Flexure modules which can be used to replace prismatic joints [17]

In existing designs both elastic hinges and flexure beams (figure 2.3a) are used as fundamental compliant members to allow motion in the mechanism. Elastic hinges (figure 2.3b) have a smaller travelling range as a result of stress concentrations at the thinnest portion of the hinge. However, the flexure beams are less stable, since buckling could occur, especially when high axial loads are applied. An overview of designs with the used flexure modules and compliant elements is shown in table 2.1.

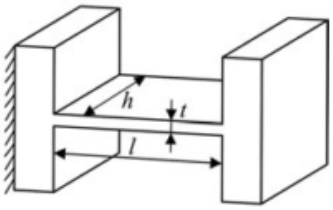

(a) Flexure beam

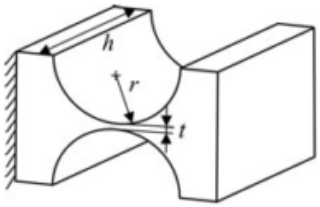

(b) Elastic hinge

Figure 2.3: Fundamental compliant members used in XY DCPMs [38]

Table 2.1: Categorization by flexures of DCPMs with two translational DOFs

	Elastic joints	flexure beams	Combination
Parallel flexure	[21, 29]	[17]	
Double parallel flexure	[27]	[1, 13, 43]	
Combination		[4, 11, 38, 46]	[25]

The parasitic rotation can be decreased by placing the centre of stiffness on the axes of actuation. Most of the mechanisms with a 4-PP structure inherently have this property since the centre of stiffness of the symmetric designs is in the middle of the motion stage. For the mechanisms with a 2-PP structure the topology has to be designed in a specific way to align the actuation axes with the centre of stiffness as shown in figure

2.4. Other parasitic motions can be decreased by increasing the out of plane stiffness of the prismatic joint flexure modules [11]. A 4-PP structure where the rigid stages between the prismatic joints in the opposite legs are rigidly connected is proposed by Yu and Hao [17, 43]. This design would further decrease the cross-axis coupling and parasitic motion of the motion stage.

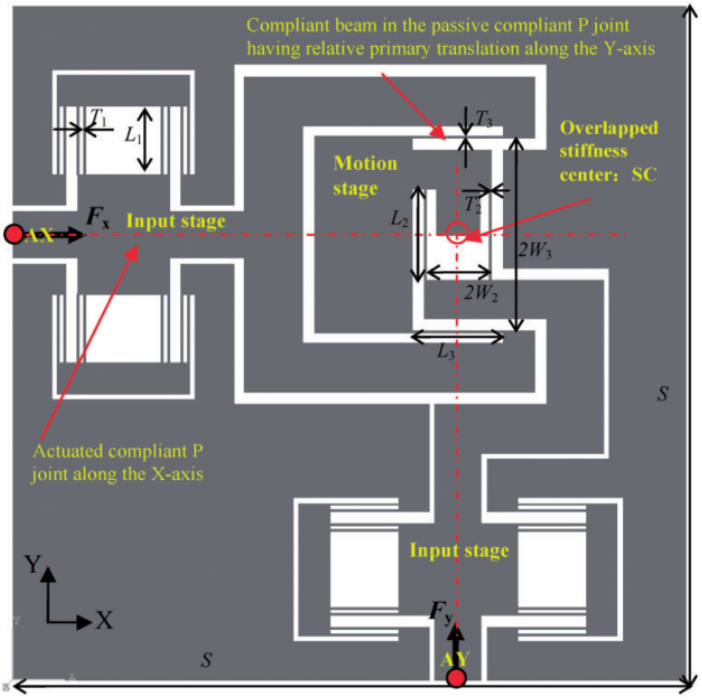

Figure 2.4: DCPM with a 2-PP structure and intersection of axes of actuation at the centre of stiffness [11]

2.2.2. Translational three degree of freedom mechanisms

Unlike most XY DCPMs which are composed using two or three PP legs the XYZ DCPMs from previous designs have a variety of kinematic designs. A simple transition is made by Hao [14] where a XYZ DCPM is designed with a 3-PPP structure. An XY DCPM from Awtar[1] is inverted and used for the two passive prismatic joints. Which are actuated through a compound parallel flexure module. Other 3-PPP designs are proposed by Awtar [2] with parallel leaf springs as prismatic joints and [39] where both compound parallel flexure modules and compound double parallel flexure modules with elastic joints are used. Similary, a 3-PPPR design is proposed by Pham [33] where an inverted $XY\theta_z$ mechanism is used as the passive PPR joint.

Using 4-beam flexure modules 3-PPPR designs are made by Hao and Li [10, 25]. The 4-beam flexure modules exist of 4 spatial wire-beams which act a a planar (PPR) joint (figure 2.5a) and when combined orthogonal as a prismatic joint(figure 2.5b). These flexure modules have a shortening effect as a result of transverse displacement. Similar solutions to the shortening effect of parallelogram flexure modules are applied. Namely, the double 4-beam [14] and a symmetric design [24].

By changing the double parallelogram flexure module to a PPR joint by orthogonally adding two elastic hinges to each leg of the double parallelogram flexure module. These modules are used as passive PPR joints in XYZ DCPMs with a 3-PPPR structure by Li and Xu [27, 28, 41].

A exact-constraint 3-PPPRR design has been proposed by Hao [16]. A double 2-beam topology is used for the passive PPRR joint as shown in figure 2.6.

The main design approach to make a decoupled mechanism is the same as for XY mechanisms. A one DOF translational stage is connected to the motion stage with a passive flexure leg which transmits the actuation displacement without restricting the other DOFs of the motion stage. Since the combination of all legs should constrain the three rotations of the motion stage the legs have a passive PP, PPR or PPRR kinematic chain. Approaches used to reduce cross-axis coupling and parasitic motion are the same as the ones used for XY DCPMs. The inherent off-axis error of flexure beams and wire beams is reduced with parasitic motion compensating flexure modules such as double parallel flexure joint, double 2-beam, and double 4-beam

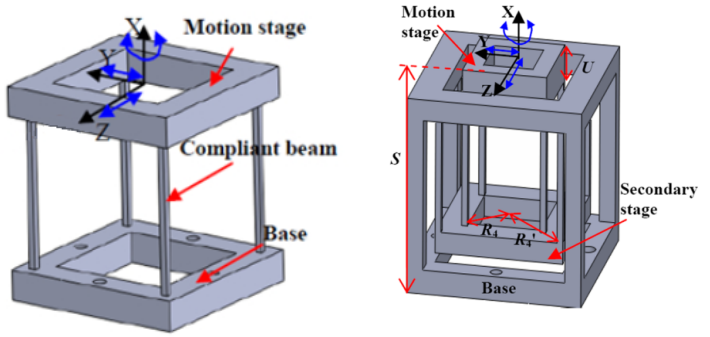

(a) 4 beam flexure module [10]

(b) Double 4 beam flexure module [14]

Figure 2.5: Flexure modules with wire beams as used for XYZ DCPMs[10, 25]

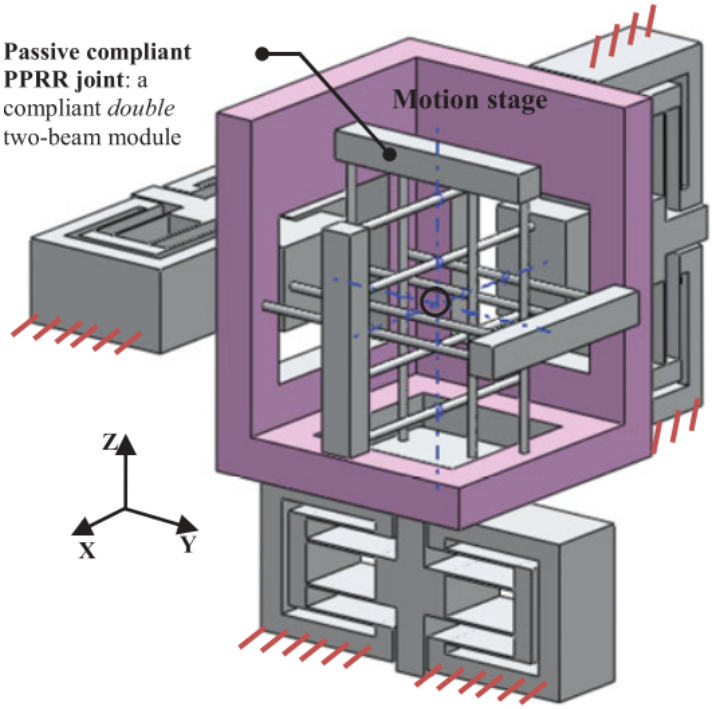

Figure 2.6: XYZ DCPM with a 3-PPPRR structure and double 2 beam flexure modules [16]

[12, 14, 16, 27, 28, 39, 41]. Unlike most XY DCPMs most XYZ DCPMs, with exeption of the design by Li [24], do not have a symmetric design which places the axes of actuation on the centre of stiffness. This can be solved by positioning the three passive kinematic chains in a specific way which makes the centres of stiffness of these chains overlap at the intersection point of the three actuations axes.

2.3. Discussion

Literature searches showed that DCPMs are extensively used in translational stages with two or three DOFs. Besides these proposed design no further DCPMs have been found which have decoupled rotational DOFs. However, kinematic architectures for decoupled spherical mechanisms have been proposed in research [7]. These architectures could be used in future work to design decoupled spherical mechanisms.

The evaluated XY DCPMs have either a 2-PP or a 4-PP structure. Mirroring a 2-PP structure to a 4-PP structure is an easy method to reduce cross-coupling and parasitic motion errors. However, this method over-constrains the mechanism and increases the volume. This means a more complex 2-PP mechanism could result in a more compact design.

There are more possible designs for the XYZ DCPMs such as the 3-PPP, 3-PPPR and 3-PPPRR structures. While the 3-PPPRR design would exactly-constrain the motion stage, the over-constrained designs might increase stability. Designs with a centre of stiffness on the actuation axes or with a symmetric topology have reduces cross-axis coupling and parasitic motion at the cost of more complexity.

Since cross-axis coupling is non-linear over the range of the mechanisms it is not possible to make a significant quantitative comparison between different mechanisms which are designed for different applications with different workspaces.

The decoupling passive flexure modules result in lost motion between the actuator and the motion stage. While some flexure modules reduce cross-axis coupling and parasitic motion better than others, they might result in more lost motion which might be undesired for control purposes.

The flexure modules which reduce the cross-axis coupling and parasitic motion have a more complex topology which might reduce manufacturability. Planar designs of the XY-stages are usually made using wire-EDM, but for spatial topologies the manufacturability has to be considered during the design process. New manufacturing methods such as additive manufacturing might allow for more design freedom for spatial DCPMs.

2.4. Conclusion

In this chapter, decoupled compliant parallel mechanisms from literature have been investigated. A wide range of XY and XYZ mechanisms was found, however not any full decoupled rotational compliant parallel mechanisms. For both the XY and XYZ mechanisms the kinematic architectures, flexure modules and compliant elements were evaluated. The XY mechanisms have either a 2-PP or a 4-PP structure. The prismatic joints are comprised of parallel flexure modules with flexure beams or elastic hinges as compliant elements. Cross-axis coupling and parasitic motion is reduced with double or compound parallel flexure modules, symmetric topologies and alignment of actuators with the centre of stiffness. The XYZ mechanisms have a 3-PPP, 3-PPPR or 3-PPPRR structure, which can also be constructed with 6 legs to achieve a symmetric topology. Flexure modules which are used are the 2-beam, 4-beam and parallel flexure modules. The cross-axis coupling and parasitic motion errors are reduced in the same way as done for XY mechanisms.

3

Design for additive manufacturing of a 4 degrees of freedom decoupled monolithic compliant alignment mechanism

Design for additive manufacturing of a 4 degrees of freedom decoupled monolithic compliant alignment mechanism

NIEK W. VAN HOEK
Delft University of Technology
niekvanhoek@gmail.com

VOLKERT VAN DER WIJK
Delft University of Technology

JUST L. HERDER
Delft University of Technology

GERRIT OOSTERHUIS
VDL Enabling Technologies Group

Abstract

This paper provides an approach to design monolithic mechanisms which can be manufactured using additive manufacturing. The approach is applied to design a monolithic optical mount with decoupled degrees of freedom (DOFs) and a high eigenfrequency. Additive manufacturing allows to design complex monolithic compliant mechanisms from high performance lightweight materials. Optical systems require adjustable mounts to align the optical components relative to a light path during installation. Depending on the application and the exact type of optical component, these mechanisms may require up to six DOFs. Such optical systems are for instance important in the semiconductor industry where high precision alignment is required for production and inspection. Decoupling of the DOFs is desired since these alignment mechanisms are often manually actuated. Four prototypes of the design are manufactured in grade 5 titanium using Laser Beam Melting. These prototypes have 4 DOFs which can be adjusted in planar translational motion with a range of 1 mm *and in rotational out of plane motion with a range of* 1 µrad *and a resolution of respectively* 10 µm *and* 10 µrad. *The four prototypes were printed without support structures and showed to be functional adjustable optical mounts. Experiments show a first eigenfrequency of* 578.1 Hz *for the best prototype.*

1. INTRODUCTION

Optical systems are applied in a growing part of industrial processes. In the semiconductor industry optical systems are required for both production and inspection of microchips. An optical system consists of a series of optical components which directs the light path going through the system. The decreasing size of details on microchips result in high requirements for positioning resolution and stability of the optical mounts which are used to align the optical components with the light path.

Conventional mechanisms [1] with sliding rigid bodies suffer from hysteresis and (virtual) play, which affects the adjustment resolution. Also, coupling between degrees of freedom(DOFs) [2] makes it difficult for the operator to tune the mount by hand to the desired position. Since optical systems can contain a multitude of optical mounts it can take a significant time to calibrate the system. Another issue is that machines with optical systems used in industrial environments are subject to vibrations. Resonance results in position errors or structural failure and should be prevented by realizing a high eigenfrequency of the mount [3].

Since compliant mechanisms have no friction, no backlash and no wear [4] they are ideal for high precision application with a high adjustment resolution. When the mechanism is manufactured

as a monolithic product there are potentially significant lower costs as a result from reduced assembly, fewer components to stock and simplified manufacturing [5]. Cumulative errors in compliant serial mechanisms result in more cross-axis coupling and parasitic motion (crosstalk) compared to parallel mechanisms which have no cumulative errors. Also, parallel mechanisms usually have low inertia and high-stiffness which results in higher eigenfrequencies [6]

However, designs for parallel compliant mechanisms often result in complex structures with a significant number of flexure elements[7][8]. The cost of manufacturing using conventional methods such as wire electrical discharge machining and milling increase with the complexity of the design. Improvements in additive manufacturing (AM) of metals result in manufacturing methods which are not affected by the complexity of the design [9]. The design freedom of AM also allows to optimize the parameters of the design to increase stiffness while staying within yield limits at maximum displacement. Significantly less material is wasted when using AM which makes the use of lightweight high performance materials such as titanium alloys relatively cheap. This increased stiffness and reduces mass would allow for designs with an high eigenfrequency.

This paper provides an approach to design monolithic mechanisms which can be manufactured by additive manufacturing of metals. This method can be used for all powder bed fusion methods and specific design rules are given for Laser Beam Melting. As an example the design of a monolithic optical mount with 4 decoupled DOFs and a high eigenfrequency is presented. Prototypes of this design are experimentally evaluated.

The design approach for AM is discussed in section 2, followed by the design of an optical mount in section 3. A finite element method for modal analysis is applied in section 4. The prototypes and experiments are discussed in section 5 and the experimental results are presented and discussed in section 5. In section 6 the applied approach is discussed and conclusions are given in section 7.

II. A COMPLIANT MECHANISM DESIGN APPROACH FOR ADDITIVE MANUFACTURING

A. Design for additive manufacturing

The most common processes for AM of metals are Laser Beam Melting (LBM), Electron Beam Melting (EBM) and Laser Metal Deposition (LMD) [10]. During LBM a thin layer of metal powder is selectively exposed to a laser beam which locally melts the material which results in solid areas. After the exposure a new layer of metal powder is applied on top of the exposed layer and the previous step is repeated to solidify powder on top of the existing solid areas. The EBM process is similar to LBM, but instead of a laser beam an electron beam is used to melt the metal powder. In LMD a surface is locally melted using a laser beam and metal powder is applied in the melt pool using a nozzle. In all the previous AM methods the structure is build on a base plate from which it is separated afterwards.
Designing for AM allows to exploit all the advantages. In this section some design considerations are presented. The design parameters are applicable for LBM and will deviate for other AM processes and materials.
LBM has a limited resolution which is defined by the laser beam diameter, powder grains size and thermal effects from the melt pool. This affects the minimum achievable wall thickness, gap size and hole diameter. Research has resulted in guidelines for minimum feature sizes which are summarized in table 1 [11, 12, 13, 14]. The minimum wall thickness is the thickness of a wall build in the build direction. Gap size is the distance between two features, but also the hole diameter of a hole in the build direction. A horizontal hole is a hole which is perpendicular to the build direction.

Table 1: *Minimum feature sizes for additive manufacturing using LBM*

Minimum wall thickness	0.4–1 mm
Minimum gap size	0.2–0.3 mm
Minimum horizontal hole diameter	0.4–1 mm

While the layer-wise process of building structures allows for more design freedom [15] it also im-

poses some limitations on the geometry of the design resulting in low surface quality and defects in the part. This can be solved by using support structures for floating and overhanging parts, but these support structures have to be removed during post processing which increases production costs. Designing with the build direction and known limitations in mind allows to profit optimally from the advantages of AM, with optimal quality of the part and minimal costs. No support structure is needed when using the design rules from table 2 [11, 16, 13, 12]. First, the maximum overhang is the distance a feature with a flat down-facing surface can extend from a vertical wall. Second, overhang angle is defined by the angle between the base plate and the down-facing surface of an overhanging feature. Finally, the maximum hole diameter is the maximum diameter of a hole perpendicular to the build direction for which is does not collapse.

Table 2: *Design rules for a self-supporting design*

Maximum overhang	0–2 mm
Minumum overhang angle	20–45°
Maximum horizontal hole diameter	7–10 mm

Even though features which meet these design rules can be made, approaching the limits won't result in an optimal quality. An overhang angle will result in a so called staircase effect which increases the surface roughness as shown in figure 1 where θ is the overhang angle. The resulting roughness can be roughly approximated by equation 1 where t is the layer thickness [9].

Figure 1: *Staircase effect of printed layers on angled features results in increased roughness [9]*

$$R_a = \frac{t \cdot \cos\theta}{4} \tag{1}$$

B. Compliant mechanism design

There are several methods to design a compliant mechanism as discussed in [17]. A kinematic approach can be used to design compliant mechanisms based on conventional rigid body mechanisms by replacing the joints with flexure joints. For this approach the location and orientation of the joints is limited when a self-supporting AM structure is desired. For example, leaf springs cannot be printed horizontally. Another kinematic approach is the Freedom and Constraint Topology approach where freedom, constraint and actuation spaces defined by screw theory are used to give the designer possible topologies for the design. However, further dimensional synthesis is required to finish the design [18, 19]. The Building blocks approach is a conceptual design procedure which uses instant centres and two different building blocks. This allows to generate an initial mechanism topology for a given input and output. The result is an initial mechanism topology and size and geometry optimization is used to generate the final design [20]. Another approach is structural optimization where the design rules are included as constraints to find a feasible solution. However, the resulting set of constraints is likely not to converge during the optimization, especially when more DOFs are required [21].

C. Eigenfrequency optimization

To obtain a design with high eigenfrequency the stiffness of the system has to be optimized. The maximum is limited by the yield strength of the flexures in the mechanism. This is done by using a finite element method to calculate the current eigenfrequencies and eigenmodes of the design. Flexures with too little stiffness in a certain direction are distinguished by analysing these eigenmodes. An optimal eigenfrequency can be found when these steps are repeated.

III. Design of an optical mount

In this case study the design approach from the previous section will be applied by designing an optical mount. The design objective is a 2-inch

concave mirror mount with an adjustment mechanism. The mechanism with 4 adjustable DOFs: 2 orthogonal translations in plane of the mirror and two tilting rotations out of plane, with adjustment ranges of 1 mrad and 1 mm with a resolution of 1 µm and 10 µrad, respectively. The axes of rotation of the tip and tilt rotations pass through the optical centre of the mirror. Since the requirements for different applications will be different a transmission mechanism is added for each adjustable DOFs. The adjustment mechanism is divided in 2 stages. The translation stage has parallel translational adjustments in X and Y direction. In series with this parallel stage is the tip-tilt stage holding the mirror which can be rotated in parallel about the X and Y axes. The DOFs are actuated using adjustments screws with a pitch of 80 threads per inch (TPI) for the translations and 508 TPI for the rotations. The proposed design for the optical mount is shown in 5.

A. Application of guidelines for AM

The guidelines defined in the previous section are applied on the proposed optical mount design from 5. The minimum wall thickness can be found at flexures 1 to 18 which is equal to 1 mm. Gaps are smallest between the rigid bodies of the tip-tilt stage, these bodies have a safe minimum distance of 1 mm. Down-facing surfaces were avoided when possible to acquire a self-supporting design. The remaining down-facing surfaces can be found at the slanted leaf springs 5 to 8 and at the down-facing notches of elastic hinges 19 to 21. The slanted leaf springs have an overhang angle of 60° and the notches have a diameter of 8 mm.

B. Topology design

A new 2 degree of freedom translational stage is proposed as shown in figure 2. This stage suspends the tip-tilt stage with two pairs of parallel leaf springs. These parallel leaf springs allow transverse motion, but have high stiffness in axial direction. These pairs of leaf springs decouple actuated DOFs, although the shortening effect of the leaf springs results in a small parasitic motion which is equal to [22]:

$$\Delta y = -0.6 \cdot \frac{(\Delta x)^2}{L} \tag{2}$$

Where Δx and Δy are respectively the transversal and axial displacement at the end of the leaf spring and L is the length of the leaf spring. This would result in a cross-axis coupling error of 24 µm at an 1 mm displacement. An axial displacement is applied by a lever mechanism which is actuated by an adjustment screw. A curved geometry prevents local stress concentrations.

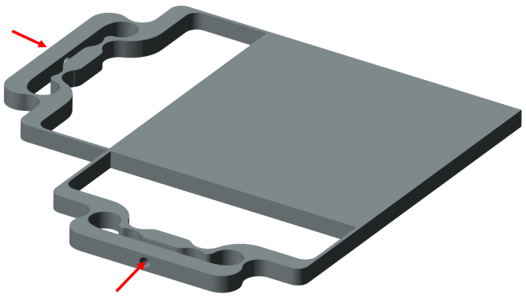

Figure 2: *Design of the translation stage with the lever mechanism which is actuated at the arrows [23]*

The tip-tilt is based on the decoupled spherical 5 bar mechanism proposed by Gosselin [24]. This mechanism as shown in figure 3 is suitable for the optical mount since it allows for rotation around the X and Y axes intersecting in the middle of the mirror. However, in the proposed configuration it is not suitable for additive manufacturing. A new design is shown in figure 4. This flat design has no floating structures and limited overhang angles. The rotational actuation is applied by a lever suspended by cross flexures. Joint 5 is replaced by an elastic hinge and joint 2 by two elastic hinges on both sides of the mirror which allow rotation around the same axis. This results in more stability of the mirror. Joint 4, which allows rotation around the Z-axis, would have to be place in front or behind the mirror to allow rotation around the Z-axis. This blocks the light on one side and blocks the user from placing the mirror on the other side. By replacing this joint with a cross-flexure rotation around the Z-axis as shown by the dashed lines in figure 4. The combination of these stages results in

the design shown in figure 5. The output rotations (φ_1, φ_2) as a function of the input rotations (θ_1, θ_2) can be calculated using equations 3 and 4 [25].

$$\phi = \theta_1 \tag{3}$$

$$\phi_1 = \arctan\left(\frac{\tan\theta_2}{\cos\theta_1}\right) \tag{4}$$

These equations show that there is no coupling error when only one rotation is actuated. However, when both rotations are actuated there is a small coupling error for φ_2.

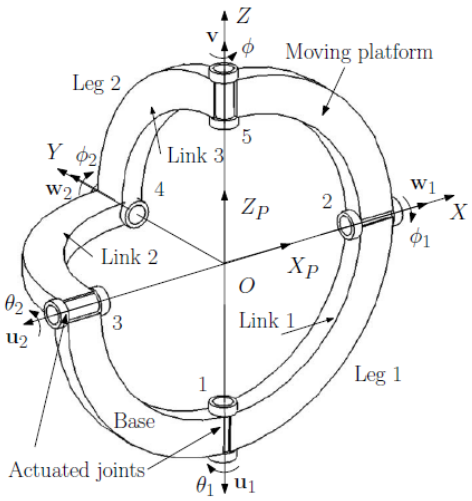

Figure 3: *A drawing of the 5 bar 2 DOF spherical mechanism with base link 1-3 and moving platform link 2-5 [23]*

C. Design of flexures

In this design a kinematic approach is applied by using flexure joints. The used flexures are leaf springs and elastic hinges. The stiffness in the allowed DOF(s) of these flexures and the corresponding maximum stresses have to be calculated to analyse and optimize the design.

Leaf springs are used in two configurations: parallel (figure 6) and crossed (figure 7). The parallel leaf springs allow transverse displacement and the cross flexure guide a rotation around the intersection point.

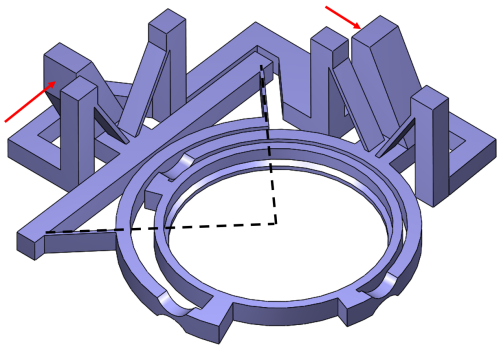

Figure 4: *Compliant design of the tip-tilt stage, where hinges 1,3 and 4 are replaced by cross-flexures and hinges 2 and 5 by elastic hinges. The mechanism is actuated at the arrows and the dashed lines show the pole of the cross-flexure which replaces hinge 4.*

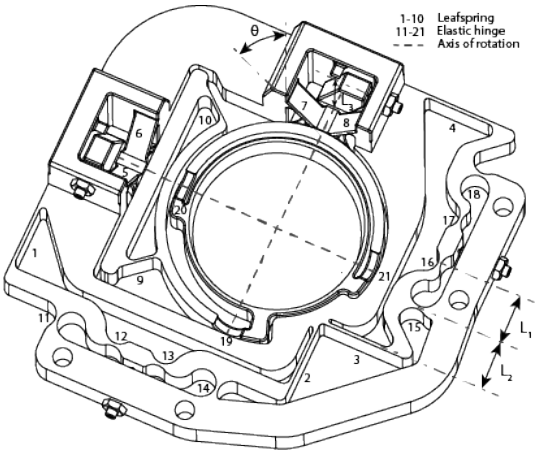

Figure 5: *Drawing of the optical mount with numbered flexures and transmission parameters.*

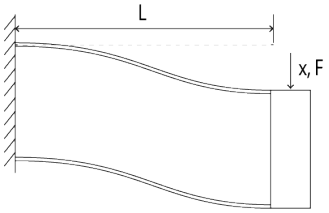

Figure 6: *Model of a deflected leaf spring with displacement (x), force (F) and length (L)*

The stiffness against a translation in x direction of the parallel leaf springs is calculated using equa-

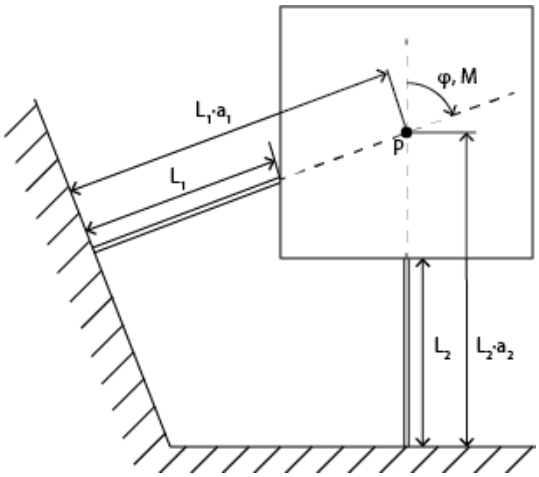

Figure 7: *Model of a cross flexure with rotation (φ), moment (M), leaf springs lengths (L_1 and L_2), pole (P) and ratio between leaf spring length and distance from fixed point to pole (a)*

tion:

$$c_x = \frac{F}{x} = 2 \cdot \frac{12 \cdot E \cdot I}{L^3} \tag{5}$$

Where F is the force applied in the direction of x, x is resulting displacement, E is the young's modulus of the used material and L is the length of the leaf spring. I is the second moment of area of the cross section of the leaf spring, which is calculated by:

$$I = b \cdot t^3/12 \tag{6}$$

Where b is the width and t is the thickness of the leaf springs. The maximum stress as a result of a deflection in x-direction is calculated with equation:

$$\sigma_{x,max} = \frac{3 \cdot E \cdot t \cdot x}{L^2} \tag{7}$$

Rotation stiffness around the pole of a cross flexure is calculated using equation 8.

$$k_\varphi = \frac{M}{\varphi} = 4 \cdot \left\{ \frac{1}{K_{z1} \cdot L_1} \cdot \left(1 - 3a_1 + 3a_1^2\right) + \frac{1}{K_{z2} \cdot L_2} \cdot \left(1 - 3a_2 + 3a_2^2\right) \right\} \tag{8}$$

Where M is the moment around the pole and φ the resulting rotation. The distance from the fixed end of the flexure and the pole is a, and K_z is the compliance vector which is equal to:

$$K_z = \frac{\left(1 - \nu^2\right)}{E \cdot I} \tag{9}$$

Where ν is the materials Poisson's ratio. The maximum stress when rotated is equal to equation[22]:

$$\sigma_{\varphi,max} = \frac{\varphi \cdot E \cdot t}{2 \cdot L} \cdot (-2 + 6 \cdot a) \tag{10}$$

This stress occurs at the fixed end of one of the leaf springs.

The width (b), thickness (t) and length (L) of the leafsprings and values of a of the cross flexures are listed in table 3.

Table 3: *Parameters of leaf springs*

Leaf spring	Length [mm]	Width [mm]	Thickness [mm]	a
1-4	25	20	1	N/A
5-8	15	7	1	1.4
9,10	10	20	1	4.5

Elastic hinges as shown in figure 8 are flexures where circular incisions result in compliance for the rotation around midpoint at the smallest intersection. The rotational stiffness is calculated using equation:

$$k_\theta = \frac{M}{\theta} = 0.093 \cdot E \cdot b \cdot h^2 \cdot \sqrt{\frac{h}{D}} \tag{11}$$

Where M is the moment around the axis of rotation and θ is the rotation. h is the minimum thickness, D is the diameter of the notches and b is the width. The maximum stiffness is equal to equation 12 from [26].

$$\sigma_{\theta,max} = 0.58 \cdot \theta \cdot E \cdot \sqrt{\frac{h}{D}} \tag{12}$$

The diameter (D), width (b) and minimum thickness (h) for all elastic hinges are listed in table 4.

The maximum displacements and rotations are respectively 1 mm and 1 mrad for the adjustable degrees of freedom which which can be used to measure the maximum stress for all flexures except the cross flexure comprised of flexure 9 and 10.

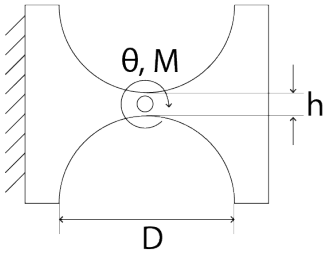

Figure 8: *Model of an elastic hinge with rotation (θ), moment (M), minimum thickness (h) and diameter (D)*

Table 4: *Parameters of elastic hinges*

Elastic hinge	Diameter [mm]	Width [mm]	Thickness [mm]
11-18	8	20	1
19-21	8	3	3

This cross-flexure allows rotation around the Z-axis which is required for the rotation around the X and Y axes. The rotation can be calculated using (13) from [23]. Using the flexure parameters and these values the stiffness and maximum stress can be calculated as shown in 5. The yield strength of Ti6Al4V Grade 5 is equal to 1100 MPa, so the maximum range can be reached without failure of the flexures.

$$R_z = \arcsin\left(\frac{\sin R_x \cdot \sin R_y}{\cos R_x \cdot \cos R_y}\right) \tag{13}$$

Table 5: *Stiffness and maximum stress of flexures made from Ti6Al4V Grade 5*

flexure	Stiffness	displacement	Maximum stress
1+2, 3+4	2.91×10^5 N m	1 mm	546 MPa
5+6, 7+8	104 N m rad^{-1}	1 mrad	23.9 MPa
9+10	8.24×10^3 N m rad^{-1}	1×10^{-3} mrad	0.142 MPa
11-18	74.8 N m rad^{-1}	1 mrad	23.3 MPa
19-21	175 N m rad^{-1}	1 mrad	40.4 MPa

D. Transmission sensitivity and resolution

The transmission sensitivity of the translational DOFs is equal to $\frac{L_1}{L_2} = 1$ as shown in figure 5. For the rotational DOFs the sensitivity is equal to:

$$S = \frac{\theta}{\Delta x} = \frac{\theta}{L_3 \cdot \tan\theta} \approx \frac{1}{L_3} \tag{14}$$

Where θ is the rotation, Δx is the input displacement and L_3 is the length of the lever. For small rotations the transmission sensitivity will be equal to L_3^{-1} which is 0.05 mm rad^{-1}. The smallest rotation a human operator could make with an adjustment screw is 1° [27]. This results in an adjustment resolution of 0.88 µm for the translational adjustments and 6.94 µrad for the rotational adjustment.

IV. Modal analysis by finite element method

Since the optical mount needs to be stable in an environment with high-frequency vibrational disturbances it needs a sufficient high first eigenfrequency. To find this eigenfrequency a finite element frequency analysis is executed using COMSOL Multiphysics 5.3a. Rigid contacts are applied between the actuated and opposite faces. A distributed load of 0.038 kg and a rigid connection are applied on flange which supports the mirror. There are some approximations in the finite element analysis. First of all, the contact sets used at the locations of the adjustment screws make the contacts bonded, although the adjustment screws only restricts motion in the direction of the adjustment screw. Secondly, the contacts are defined as surface contacts instead of point contacts. Lastly, the mass of the mirror is a distributed load on the flange only, which results in a different inertia than the real mirror. The results are used to evaluate the design and improve for an higher eigenfrequency. The final eigenfrequencies up to 1.5 kHz are shown in table 6 and the first 4 eigenmodes are shown in figure 9. The first eigenfrequency occurs at 771.5 Hz, while 500 Hz would be sufficient for semiconductor production line environments.

Table 6: *Eigenfrequencies up to 1500 Hz found in finite element analysis*

Mode	1	2	3	4	5	6
Frequency [Hz]	770.5	817.3	950.7	1049.7	1200.4	1302.1

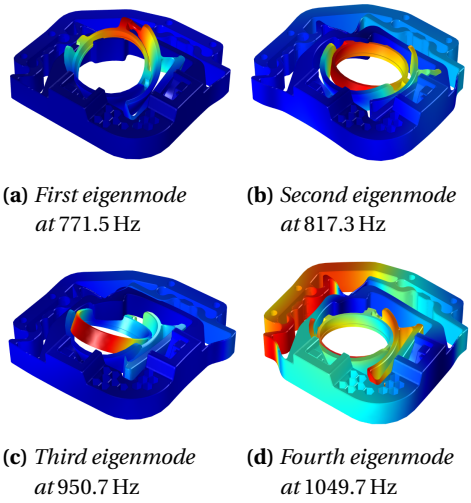

(a) *First eigenmode at* 771.5 Hz **(b)** *Second eigenmode at* 817.3 Hz

(c) *Third eigenmode at* 950.7 Hz **(d)** *Fourth eigenmode at* 1049.7 Hz

Figure 9: *The first four eigenmodes of prototype 1 determined using finite element analysis*

V. Prototypes and Experimental Setup

A. Production of prototypes

Four prototypes were made of the design and three variations. In these variations different versions of the flexures with down-facing surfaces are used to see what the surface quality is of different geometries. Flexures which are further away from the limits as presented in table 2 are expected to have better surface quality. The following designs are made:

1. Prototype 1: Design as shown in figure 5 with elastic hinges 19, 20 and 21 as shown in figure 10a and leaf springs 5, 6, 7 and 8 with an overhange angle of 60°.
2. Prototype 2: Elastic hinges 19, 20 and 21 are replaced by elastic hinges with a notch only on one side with half the diameter of the original elastic hinge as shown in figure 10b.
3. Prototype 3: Leaf springs 5, 6, 7 and 8 are under an angle of 45 degrees.
4. Prototype 4: Elastic hinges 19, 20 and 21 are replaced by elastic hinges with V-shaped notches as shown in figure 10c.

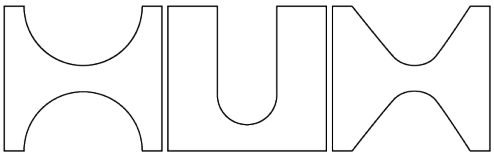

(a) *Circular elastic hinge* **(b)** *Asymmetric elastic hinge* **(c)** *V-shaped elastic hinge*

Figure 10: *Variations of elastic hinges as used in the prototypes for flexure 19, 20 and 21*

The prototypes were made from Ti6Al4V Grade 5 using LBM. They received standard stress relieve heat treatment and a beat blasting treatment. Picture 11 shows the result of prototype 1. Visual inspection shows a good result without any defects, only some roughness as would be expected from LBM. The different elastic hinges used in prototype 1, 2 and 4 are shown in figure 12. The down facing circular hinge from picture 12a is slightly collapsed in the middle. The V-shaped hinge in picture 12c does not show any clear irregularities and the asymmetric hinge from picture 12c does not have a down facing surface.

Leaf springs 7 and 8 of prototype 1 and 3 are shown in figure 13. All sloping leaf springs show a fringe near the top around the height of the main body of the optical mount. The difference in roughness between the leaf springs in picture 13a and 13b seems to be minimal.

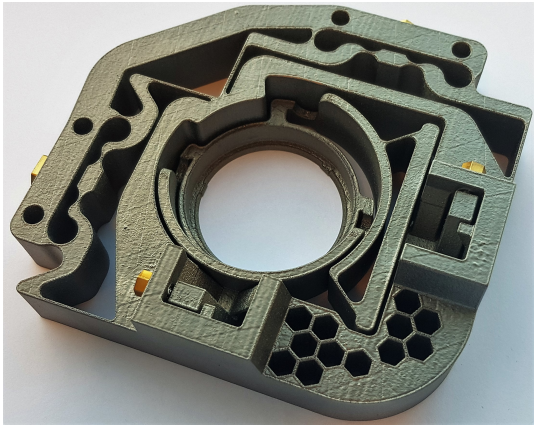

Figure 11: *Picture of the printed optical mount with some surface roughness as a result from printing and small irregularities on the tilted leaf springs.*

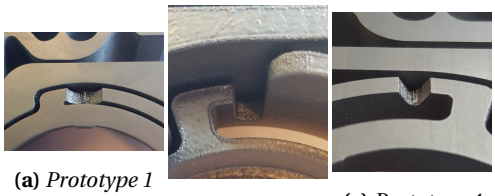

(a) *Prototype 1* **(b)** *Prototype 2* **(c)** *Prototype 4*

Figure 12: *Resulting elastic hinge 19 in prototypes 1, 2 and 4, which are respectively variations a, b and c from figure 10*

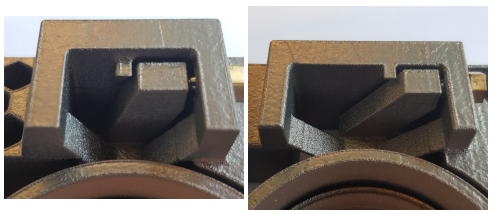

(a) *Prototype 1* **(b)** *Prototype 3*

Figure 13: *Leaf springs 7 and 8 in prototype 1 and 3 respectively a* 60° *and* 45° *overhang angle*

B. Measurement setup for modal analysis

To measure the frequency response the mechanism is excited using an Brüel & Kjaer type 4809 electrodynamic shaker and the excitation force is measured using a PCB Model 288D01 mechanical impedance sensor. The resulting displacement is measured with a Polytec PSV-400 scanning laser doppler vibrometer which measures the displacements over the entire surface of the optical mount. An elaborate description of the measurements can be found in appendix **??**.

C. Measurement setup for crosstalk analysis

To measure crosstalk between the actuated DOFs and the other DOFs the changes for each DOF are measured. This is done by measuring on 3 orthogonal planes with 1, 2 and 3 triangulating distance sensors as shown in figure 15. The mirror is replaced by a measurement tool with 3 orthogonal planes and arms to allow for more distance between measurement points. The resulting measurements are processed to the determine the change in position and orientation after actuation of one DOF. An elaborate description of the measurements can be found in appendix **??**.

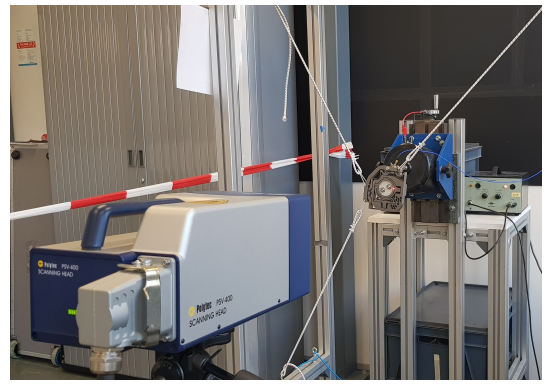

Figure 14: *A picture of the setup for experimental modal analysis with the optical mount suspended in elastic rope*

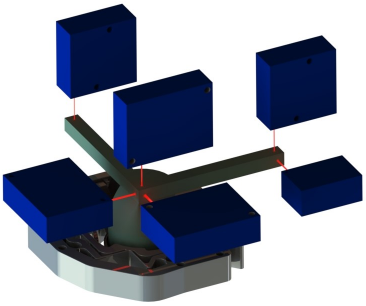

Figure 15: *Measurement setup to measure 6 DOFs with 6 triangulating distance sensors*

VI. Results

A. Experimental modal analysis

The resulting transfer function of prototype 2 is in shown in figure 17. During this measurement the adjustment screws just touch the actuation point. When the adjustment screws are turned further the peaks of the response function move to higher frequencies as can be seen in figure 18. Examination of the eigenmodes shows that the first peaks up to 40 Hz result from rigid body modes.

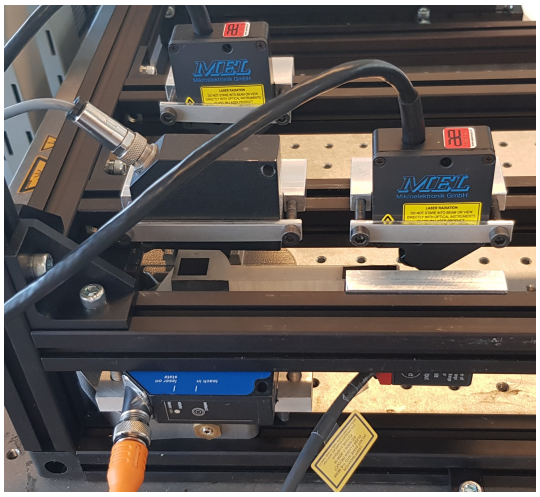

Figure 16: *A picture of the setup for crosstalk measurement with the optical mount and sensor mounted on optical rails*

The elastic eigenmodes of prototypes 1, 2 and 3 are shown in table 7 and the first four eigenmodes are shown in figure 19.

When comparing the results for prototype 1 with the results from the finite element analysis it is clear that there are quite some differences. This could be because the setup for the modal analysis has a single input and only the displacement and velocity in one direction is measured. This means an eigenmode could be missed when it is not excited by the used input vibration. If an eigenmode results in in plane displacements this mode will not show up in the measurement results. Also, the modes are manually extracted from the frequency response, if the amplitude is very small it isn't visibly recognisable in the bode plot. Another possibility is that the approximations in the finite element analysis result in higher eigenfrequencies.

Table 7: *Measured eigenfrequencies*

Mode	1	2	3	4	5	6	7
Prototype 1 [Hz]	568.8	684.4	858.8	970.0	1061	1199	1473
Prototype 2 [Hz]	578.1	652.5	848.1	928.1	1116	1238	1413
Prototype 3 [Hz]	521.9	683.8	841.9	915.6	1178	1372	1467

B. Crosstalk measurement

The resulting translations and rotations from the crosstalk measurements are shown in figures 20a, 20b, 20c and 20d. On the X-axis is the displacement or rotation of the adjusted DOF, on the left Y-axis are the resulting non-actuated translations and on the right Y-axis are the resulting non-actuated rotations.

VII. Discussion

AM proves to be a good tool to make compliant mechanisms. However, it is recommended to design them in such a way that no support structures are required. To design them without support structures some rules have to be followed. Flexures such as wire beams and leaf springs can not be printed in horizontal orientation. As a result numerous existing compliant mechanism design can not be made using AM without support structures. This poses a challenge to find solutions when parallel mechanisms with more DOFs are required.

During this research a solution was found by separating the mechanism in two stages with two DOFs. Another approach could be to find alternatives for these standard flexures which are self-supporting.

The design rules provided in this paper are based on previous research, which apply different classifications. Failure is defined by the amount of roughness or disfigurements on the feature. Because of this uncertainty the designer should try to have a safety margin from these limits. Also, the effect of the roughness on the performance of flexures was not investigated in this work. Better defined design rules and more insight on the effect of roughness would allow the designer to improve the design.

A few improvements could be made to reduce the crosstalk in the optical mount. By using parasitic motion compensation the off axis displacement caused by the parallel leaf springs could be resolved. Also, the current point of actuation for the translations results in a rotation since it imposes a moment on the leaf springs. This would be resolved when the line of actuation is through the middle of the leaf springs.

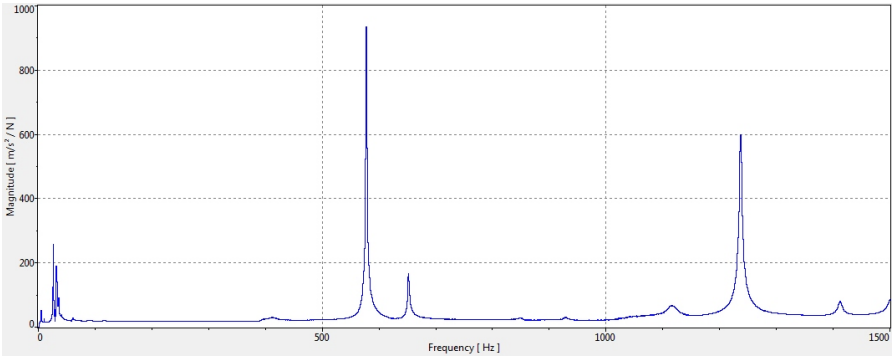

Figure 17: *The magnitude of the frequency response of prototype 2 without actuation plotted over the frequencies between* 0–1.5 kHz.

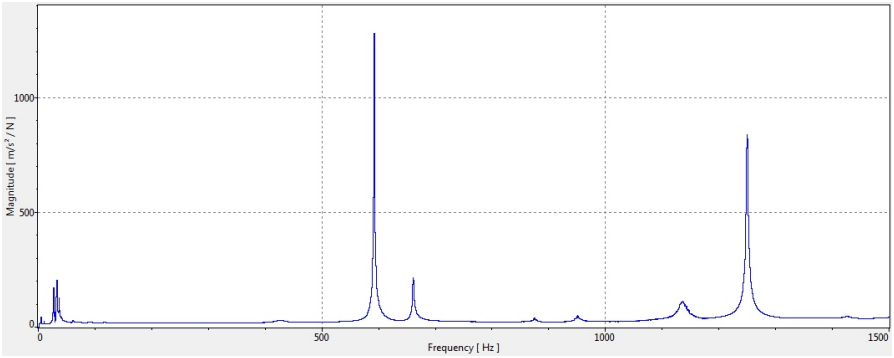

Figure 18: *The magnitude of the frequency response of prototype 2 when actuated plotted over the frequencies between* 0–1.5 kHz.

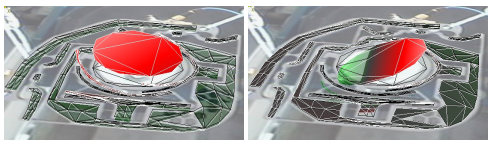

(a) *First eigenmode at* 578.1 Hz

(b) *Second eigenmode at* 652.5 Hz

(c) *Third eigenmode at* 848.1 Hz

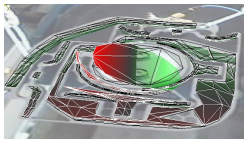

(d) *Fourth eigenmode at* 928.1 Hz

Figure 19: *Experimental modal analysis results of the first 4 eigenmodes of prototype 1*

The parameters of the flexures could be further optimized. Higher stiffness would result in higher eigenfrequencies and also higher stresses when actuated. However, from table 5 it can be seen that there is still a margin for the stress to increase.

The high stiffness of the parallel leaf springs makes it hard to make precise adjustments when rotating the adjustment screws. Also, the selected adjustment screws had to be able to allow for high axial load. This meant that it was not possible to use adjustment screws with a high resolution, although the used adjustment screws still have sufficient resolution for the requirements of this optical mount.

Eigenfrequencies obtained by finite element analysis are higher than the measured eigenfrequencies. This could be a result of the limited resolution of AM which causes dimensional errors of the flexure elements. Also, a layer of approximately 0.7 mm was removed from the bottom when the

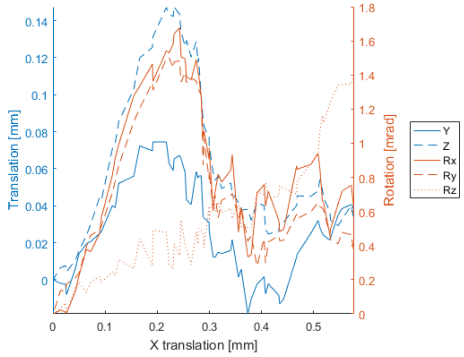

(a) *Crosstalk resulting from translational adjustment in X-direction*

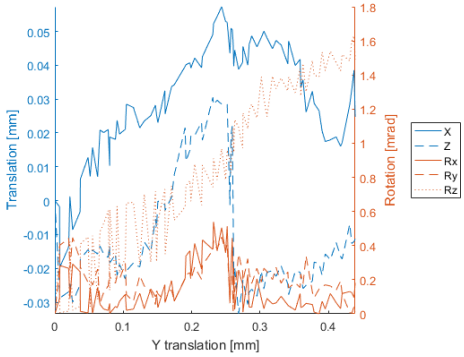

(b) *Crosstalk resulting from translational adjustment in Y-direction*

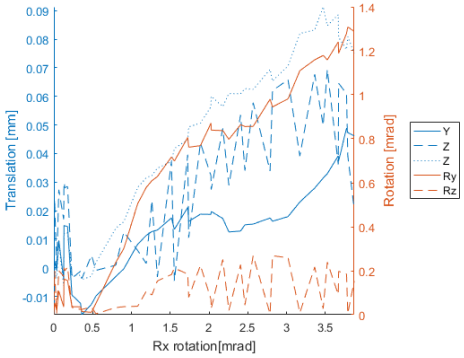

(c) *Crosstalk resulting from rotational adjustment around the X-axis*

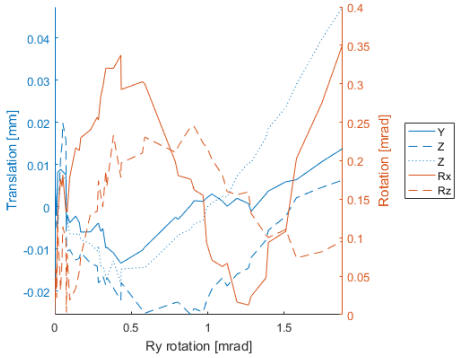

(d) *Crosstalk resulting from rotational adjustment around the Y-axis*

Figure 20: *Crosstalk measurement results of prototype 2*

mechanism was detached from the building plate. On the other hand, this could also be a result of modelling approximations made in the finite element model, since the adjustment screws were modelled as connected planes and the mass of the mirror is modelled as a distributed load on the flange which supports the mirror. The eigenmode shown in figure 9d results in translations in plane of the adjustable axis which does not show up in the measurements.

The translation of X and Y both result in a parasitic rotation around the Z-axis as shown in figures 20a and 20b. Since the axes of actuation do not intersect at the centre of stiffness of the translation stage a moment is exerted on the parallel leaf springs which results in this rotation.This could be solved by positioning the adjustment screws such that their axes of actuation intersect the leaf springs at halfway their length [22]. Both translational adjustments result in parasitic motion in Z-direction with a maximum of 150 µm at 200 µm displacement in X-direction. This could be improved by increasing the out of plane stiffness.

The crosstalk measurements of the rotations around the X and Y axes both show a parasitic translation in Z direction and cross-axis coupling to the other rotation. Since the decoupling elastic-hinges have a significant rotational stiffness they do not fully decoupled the mechanism. The crosstalk could also be reduced by mirroring the mechanism by placing passive cross-flexure on the opposite sides of the stage.

VIII. Conclusion

An approach to design compliant mechanisms for additive manufacturing is proposed with a set of design rules. This approach was used in a case study for a new design of an optical mount with 4 decoupled degrees of freedom. Four prototypes of this design with each having slight differences, were manufactured from grade 5 titanium using Laser Beam Melting, showed to be functional adjustable optical mounts. Experiments have shown a first eigenfrequency of 578.1 Hz for the best prototype which is more than sufficient for the current machines in the semiconductor industry. The crosstalk was evaluated and showed rotation around the Z-axis as a result of X and Z translation. Tip and tilt show coupling up to 1.3 mrad at a rotation around the X-axis of 4 mrad. Unexpected out of plane displacements and rotations of 0.15 mm and 1.8 mrad appeared at 0.2 mm displacement in X-direction. These results confirm the viability of the proposed approach to design high precision monolithic compliant mechanisms.

References

[1] A. Y. Dallakian, "Gimballed optical mount," 2001.

[2] E. T. Kvamme and M. T. Sullivan, "A small low-stress stable 3-dof mirror mount with one arc-second tip/tilt resolution," in *Space Systems Engineering and Optical Alignment Mechanisms*, vol. 5528, pp. 264–272, International Society for Optics and Photonics, 2004.

[3] S. S. Rao and F. F. Yap, *Mechanical vibrations*, vol. 4. Prentice Hall Upper Saddle River, 2011.

[4] T. J. Teo, G. Yang, and I.-M. Chen, "Compliant manipulators," in *Handbook of Manufacturing Engineering and Technology*, pp. 2229–2300, Springer, 2015.

[5] L. L. Howell, S. P. Magleby, and B. M. Olsen, *Handbook of compliant mechanisms*. John Wiley & Sons, 2013.

[6] C.-X. Li, G.-Y. Gu, M.-J. Yang, and L.-M. Zhu, "Design, analysis and testing of a parallel-kinematic high-bandwidth xy nanopositioning stage," *Review of Scientific instruments*, vol. 84, no. 12, p. 125111, 2013.

[7] H. Li, G. Hao, and R. C. Kavanagh, "A new xyz compliant parallel mechanism for micro-/nano-manipulation: Design and analysis," *Micromachines*, vol. 7, no. 2, p. 23, 2016.

[8] G. Hao and H. Li, "Conceptual designs of multi-degree of freedom compliant parallel manipulators composed of wire-beam based compliant mechanisms," *Proceedings of the Institution of Mechanical Engineers, Part C:*

Journal of Mechanical Engineering Science, vol. 229, no. 3, pp. 538–555, 2015.

[9] L. Yang, K. Hsu, B. Baughman, D. Godfrey, F. Medina, M. Menon, and S. Wiener, *Additive Manufacturing of Metals: The Technology, Materials, Design and Production*. Springer, 2017.

[10] D. Herzog, V. Seyda, E. Wycisk, and C. Emmelmann, "Additive manufacturing of metals," *Acta Materialia*, vol. 117, pp. 371–392, 2016.

[11] D. Thomas, *The development of design rules for selective laser melting*. PhD thesis, University of Wales, 2009.

[12] G. A. Adam and D. Zimmer, "On design for additive manufacturing: evaluating geometrical limitations," *Rapid Prototyping Journal*, vol. 21, no. 6, pp. 662–670, 2015.

[13] Crucible, "Design guidelines for direct metal laser sintering (dmls)," 2015.

[14] Renishaw, "Design for metal am - a beginner's guide," August 2017.

[15] R. Hague, I. Campbell, and P. Dickens, "Implications on design of rapid manufacturing," *Proceedings of the Institution of Mechanical Engineers, Part C: Journal of Mechanical Engineering Science*, vol. 217, no. 1, pp. 25–30, 2003.

[16] G. A. Adam and D. Zimmer, "Design for additive manufacturing-element transitions and aggregated structures," *CIRP Journal of Manufacturing Science and Technology*, vol. 7, no. 1, pp. 20–28, 2014.

[17] J. A. Gallego and J. Herder, "Synthesis methods in compliant mechanisms: An overview," in *ASME 2009 International Design Engineering Technical Conferences and Computers and Information in Engineering Conference*, pp. 193–214, American Society of Mechanical Engineers, 2009.

[18] J. B. Hopkins and M. L. Culpepper, "Synthesis of multi-degree of freedom, parallel flexure system concepts via freedom and constraint topology (fact)–part i: Principles," *Precision Engineering*, vol. 34, no. 2, pp. 259–270, 2010.

[19] J. B. Hopkins, *Design of flexure-based motion stages for mechatronic systems via freedom, actuation and constraint topologies (FACT)*. PhD thesis, Massachusetts Institute of Technology, 2010.

[20] C. J. Kim, S. Kota, and Y.-M. Moon, "An instant center approach toward the conceptual design of compliant mechanisms," *Journal of Mechanical Design*, vol. 128, no. 3, pp. 542–550, 2006.

[21] P. Smorenberg, "Towards topology optimization for constructing compliant optical mount mechanisms by means of additive manufacturing," 2017.

[22] H. Soemers, *Design Principles for precision mechanisms*. T-Pointprint, 2011.

[23] X. Kong, "Forward displacement analysis and singularity analysis of a special 2-dof 5r spherical parallel manipulator," *Journal of Mechanisms and Robotics*, vol. 3, no. 2, p. 024501, 2011.

[24] C. M. Gosselin and F. Caron, "Twodmount-of-freedom spherical orienting device," 1999.

[25] L. D. P. M. e. a. Samson, E., "The agile stereo pair for active vision," *Machine Vision and Applications*, 2006.

[26] M. P. Koster *et al.*, *Constructieprincipes voor het nauwkeurig bewegen en positioneren*. Universiteit Twente, 1996.

[27] K. J. Kasunic, *Optomechanical systems engineering*. John Wiley & Sons, 2015.

4

Discussion

Some of the results from the investigation of previous research in chapter 2 have been applied in the design of the optical mount. The translation is suspended by parallel leaf springs which act as a passive prismatic joint to allow transverse displacement. This method is often applied in decoupled compliant parallel XY mechanisms. In the proposed rotation stage the tip and tilt of the stage is actuated through passive elastic hinges which allow rotation around the orthogonal axis of rotation. However, the results from the crosstalk measurements still show cross-axis and parasitic motion errors. The design approaches discussed in chapter 2 which have been used in previous research to reduce these errors could be applied to improve the current design.

First, by using double parallel leaf springs the shortening effect would be resolved in the translation stage. Second, positioning the actuators on axes which intersect at the centre of stiffness reduces parasitic rotation. And finally, both stages could be improved by adding passive kinematic chains which result in a symmetric design. By adding these improvements in future research the crosstalk errors could be reduced. Although, the double parallel leaf springs have under-constraint bodies which could reduce the dynamic performance of the system and the symmetric design would significantly increase the volume and mass which reduces the dynamic performance as well.

This study showed that AM is a viable manufacturing method for decoupled compliant parallel mechanisms. When we look at previous designs the XY mechanisms have a planar topology which is ideal for wire EDM, but also easy to manufacture using AM since no support structures are needed and the limited height reduces manufacturing time. However, the current XYZ mechanism designs are not suitable for AM since their spatial topology requires a lot of support structures. By satisfying the minimum feature sizes and overhang constraints as indicated in the proposed design approach, suitable topologies will be achieved.

5

Conclusion

A new design approach for additive manufacturing of decoupled compliant parallel mechanisms was proposed in this thesis. This design approach is composed of design rules and considerations which allow for additive manufacturing of mechanisms without support structures and sufficient surface quality. The thickness of thin features which allow motion between rigid-bodies is limited and the build direction has to be kept in mind since overhanging features are bound to dimensional constraints for a self supporting structure. Overhang can not always be avoided when compliance in the build direction is required. In this case the proposed design rules are applied as is done for the elastic joints and cross flexures of rotation stage of the optical mount.

An investigation was conducted into decoupled compliant parallel mechanisms. The mechanisms found in literature were categorized by their degrees of freedom and their kinematic architecture, flexure modules and compliant elements were evaluated. Furthermore, design approaches to reduce cross-axis coupling and parasitic motion were highlighted. From this investigation it was concluded that although a number of XY and XYZ decoupled compliant parallel mechanisms are found in literature, no significant research has been done on rotational mechanisms. The topologies of the XY mechanisms are suitable for additive manufacturing, while the spatial topology of the XYZ mechanisms requires a lot of support structures when manufactured using additive manufacturing.

A new 4 degree of freedom decoupled monolithic compliant optical mount was designed. This mount is comprised of two stages with respectively two translational and two rotational degrees of freedom. For the design of the translation stage the 2-PP kinematic architecture from XY mechanisms from literature was used. Since no literature was found on rotational decoupled compliant parallel mechanisms a novel tip tilt mechanism was proposed. The flexure parameters of the mechanism were optimized for a high eigenfrequency while constraint by the yield stress at maximum range and the design rules for additive manufacturing. A first eigenfrequency of 578.1 Hz was achieved.

Four prototypes with variations of flexure elements are made from Ti6Al4V grade 5 using Laser Beam Melting. The eigenfrequencies and crosstalk of the prototypes are experimentally validated. This proved that additive manufacturing is a viable method to produce high precision compliant mechanisms.

A

Experimental modal analysis

In experimental modal analysis the natural frequencies are determined through vibration testing. This is based on the idea that the response of a system exhibits a sharp peak when the applied vibrational frequency is equal to the natural frequency [34]. By exciting the system with a signal containing a range of frequencies a complete dynamic description can be obtained. This appendix gives a discription of the experimental modal analysis and the results.

A.1. Experimental setup

The measured system has to be suspended with relatively low stiffness, such that the rigid-body modes are easy to distinguish in the results. Hardware used for modal analysis consists of excitation, measurement and data processing equipment

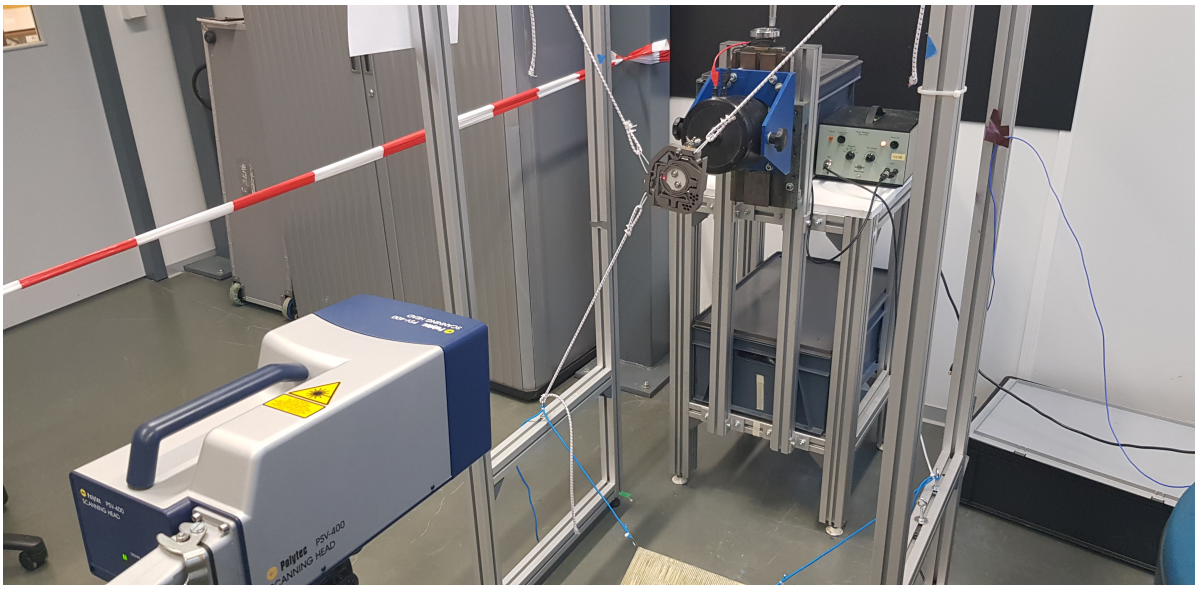

Figure A.1: A picture of the experimental modal analysis setup

A.1.1. Excitation

Excitation of the system can be done using a excitation hammer or a shaker. In this case a electrodynamic shaker (Brüel & Kjaer) is used for excitation. The shaker is connected to the mechanism via a stringer, this is a thin metal rod which only transfers axial forces and isolates the shaker. The shaker provides a pseudo random signal.

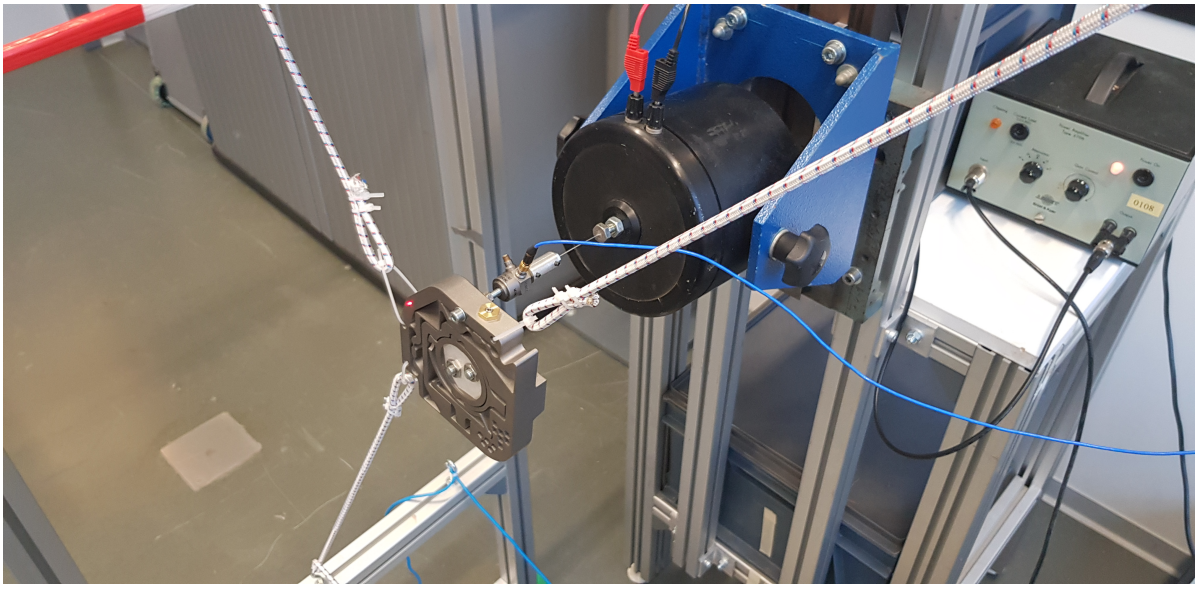

Figure A.2: A close up picture of the experimental modal analysis setup

A.1.2. Measurement

The find the frequency response two values need to be measured. The input force and the resulting vibration. The input force can be measured using a force transducer. This force transducer has to be connected between the stinger and to only measure the forces which are applied on the mechanism.

The displacements are measured using a scanning laser doppler vibrometer. This measement device exploits the doppler effect to calculate the displacement and velocity using the doppler frequency shift when light reflects from a moving object.

A.1.3. Data processing

The signals from the vibrometer and force transducer in time domain are converted to digital frequency-domain data using a Fast Fourier Transform (FFT). The resulting frequency-response functions are sent to a computer where the data can be visualized.

A.2. Results

Measurements are made of prototype 1, 2 and 3. Each prototype is measured in two settings. In the first setting the adjustment screws just touch the point of actuation and in the second setting all adjustment screws are actuated by 1.5 revolution. This results in an actuation of 0.572 mm for the translational adjustments and 3.75 mrad for the rotational adjustments. This significantly increases the stresses in the mechanism.

Table A.1: Measured eigenfrequencies of the 3 prototypes in non-actuated and actuated setting

Mode	1	2	3	4	5	6	7
Prototype 1 [Hz]	568.8	684.4	858.8	970.0	1061.3	1199.4	1473.1
Prototype 1 actuated [Hz]	583.8	688.1	881.3	981.9	1083.1	1223.8	1367.5
Prototype 2 [Hz]	578.1	652.5	848.1	928.1	1115.6	1237.5	1412.5
Prototype 2 actuated [Hz]	592.5	661.3	875.6	951.3	1136.9	1250.0	1426.9
Prototype 3 [Hz]	521.9	683.8	841.9	915.6	1178.1	1371.9	1466.9
Prototype 3 actuated [Hz]	538.1	688.8	861.9	925.0	1183.8	1411.3	1483.8

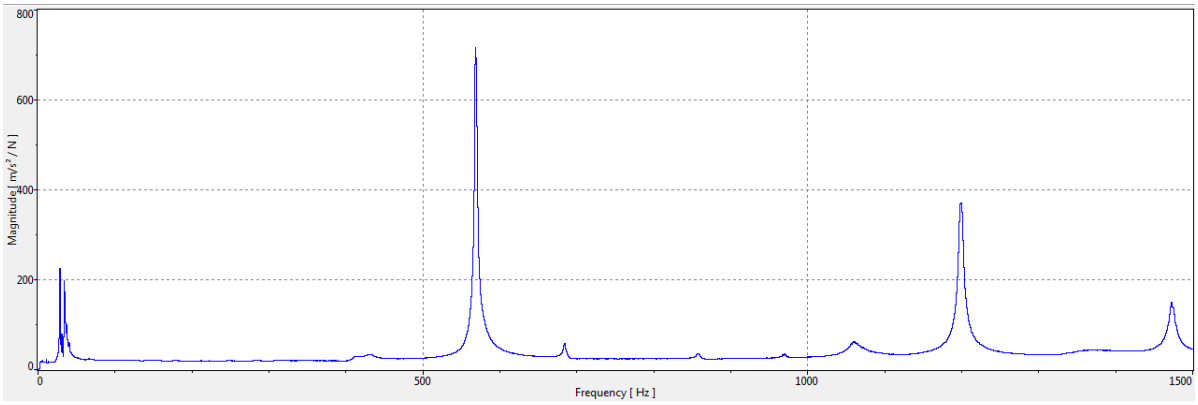

Figure A.3: The magnitude of the frequency response of prototype 1 without actuation plotted over the frequencies between 0 kHz to 1.5 kHz.

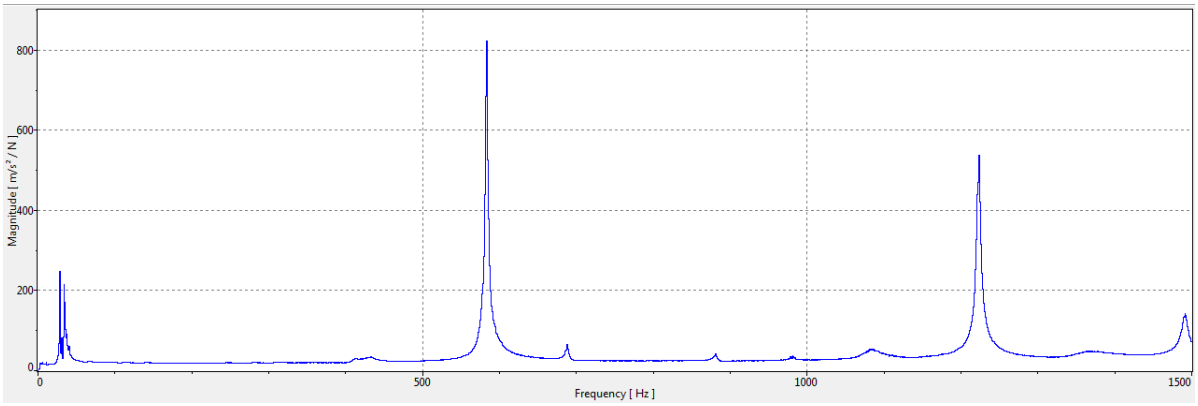

Figure A.4: The magnitude of the frequency response of prototype 1 when actuated plotted over the frequencies between 0 kHz to 1.5 kHz.

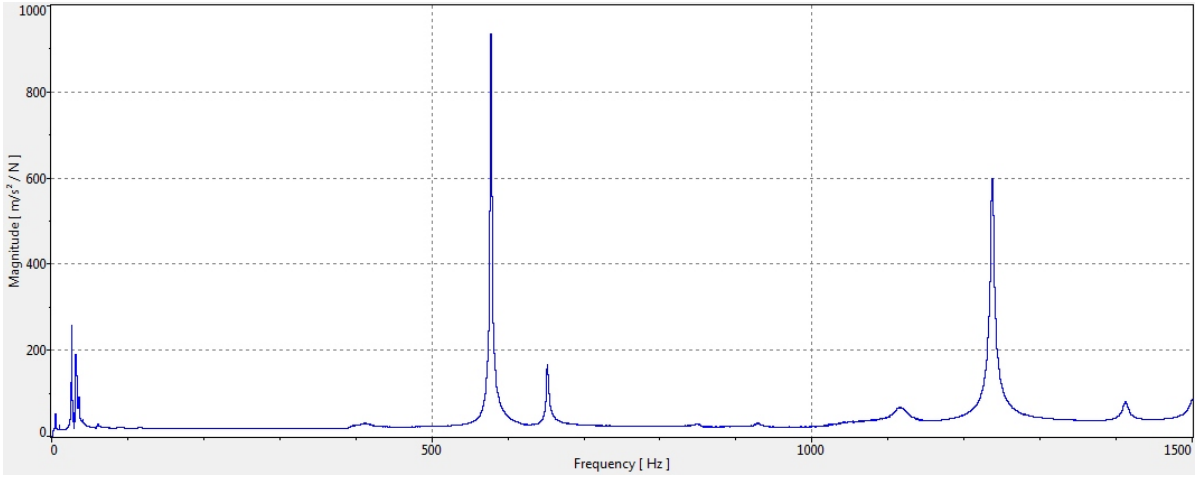

Figure A.5: The magnitude of the frequency response of prototype 2 without actuation plotted over the frequencies between 0 kHz to 1.5 kHz.

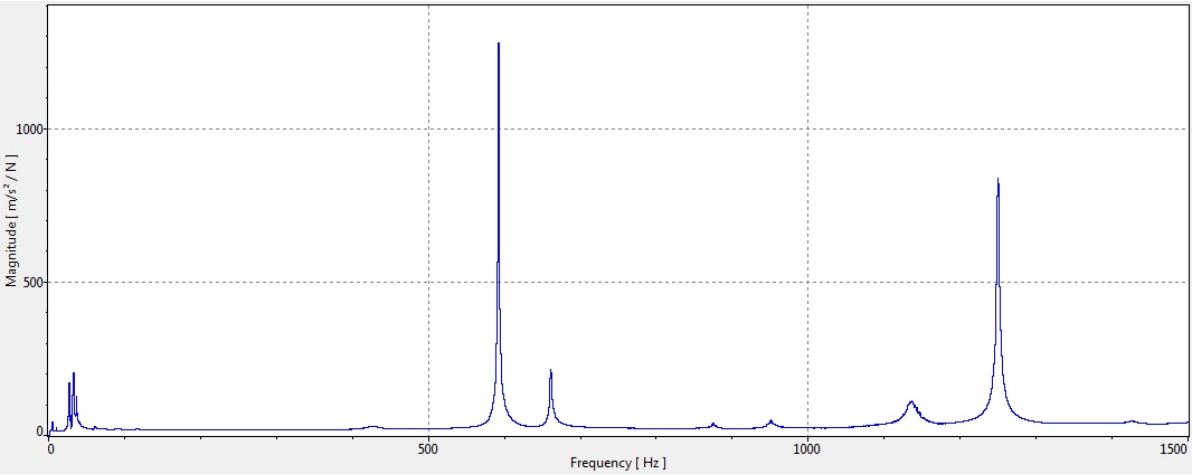

Figure A.6: The magnitude of the frequency response of prototype 2 when actuated plotted over the frequencies between 0 kHz to 1.5 kHz.

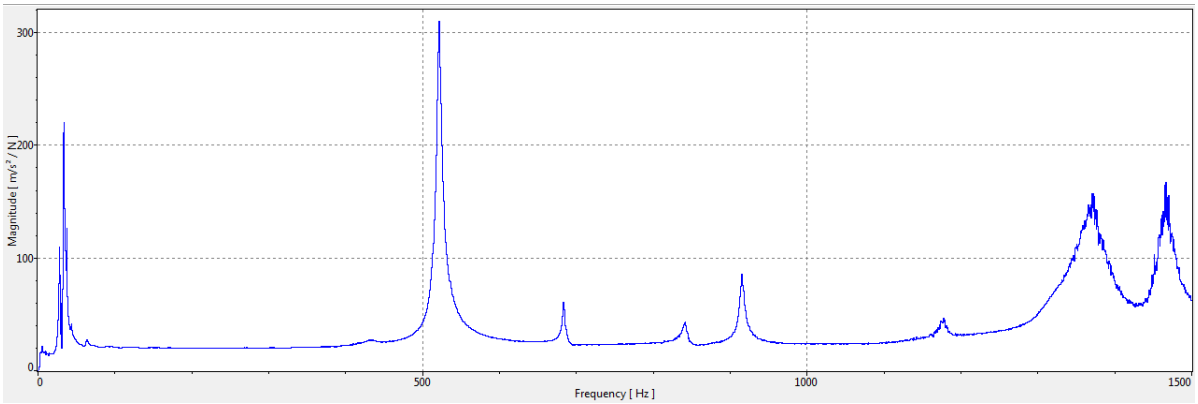

Figure A.7: The magnitude of the frequency response of prototype 3 without actuation plotted over the frequencies between 0 kHz to 1.5 kHz.

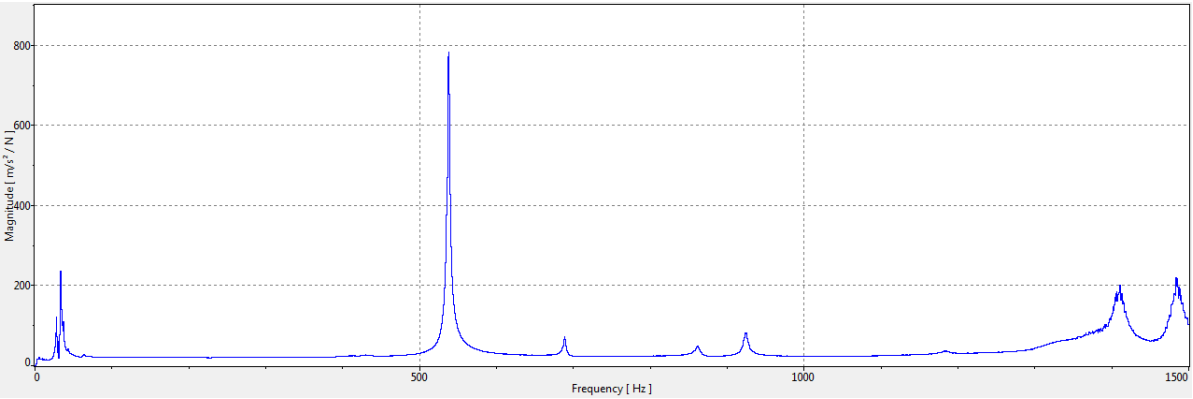

Figure A.8: The magnitude of the frequency response of prototype 3 when actuated plotted over the frequencies between 0 kHz to 1.5 kHz.

B

Crosstalk measurement

B.1. Introduction

Crosstalk is the motion of other degrees of freedom (DOFs) in response to the displacement of the actuated DOF. An adjustment mechanism with high crosstalk would require more adjustment iterations to converge to the desired position. The optical mount discussed in the paper has 4 DOFs, for each of these DOFs the displacement of all 5 other DOFs should be measured as a result of an adjustment. The position is defined by the x, y and z translation of the optical centre of the mirror. The rotation is defined by the rotation around the optical centre at the current position of the optical centre with respect to the original orientation.

B.2. Experimental setup

The position and orientation of the mirror will be measured using 6 distance sensors. Since 3 planes have to be defined there are respectively 1, 2 and 3 measurement points on these planes. Measuring the mirror directly is not possible since it only allows for measurements from the top or bottom. Instead, the mirror is replaced by a measurement tool which is shown in figure B.1.

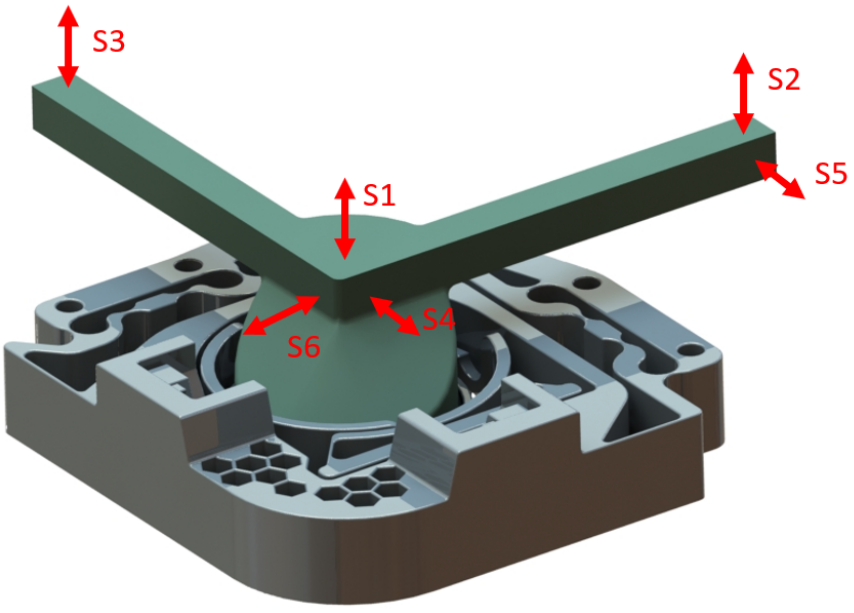

Figure B.1: A printable measurement tools with 3 planes which are defined by 6 measurement points

The displacement at the measurement points in the direction normal to the plane is measured by 6 distance sensors. The sensors used for this are triangulation distance sensors as shown in table B.1. This results

Table B.1: Used sensors and corresponding measurement range and resolution

Sensor	Brand	Model	Range [mm]	Resolution [µm]
S1	Micro-Epsilon	ILD 1401-5	5	0.6
S2	wenglorMEL	M7L-10U/0.5	0.5	0.2
S3	wenglorMEL	M7L-10U/0.5	0.5	0.2
S4	Micro-Epsilon	ILD 1402-10	10	1
S5	Micro-Epsilon	ILD1420-10	10	0.5
S6	Micro-Epsilon	ILD1401-10	10	1

in the measurement setup as shown in figure B.2. The optical mount and sensors are positions using a frame build from optical rails and milled aluminium sensor clamps as shown in figure

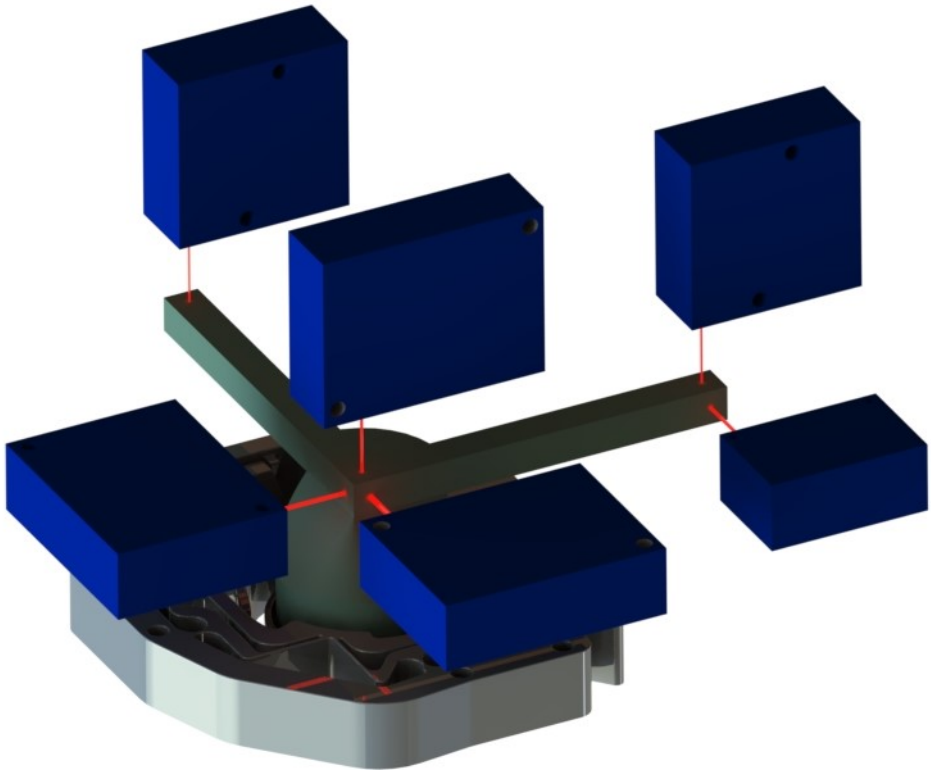

Figure B.2: The measurement setup including sensor placement

B.2.1. Data analysis

The 6 measurements can be used to define three planes by the normal vector $\mathbf{n_i}$ and the normal distance D_i to the origin O using equations B.1

$$\begin{aligned}
\mathbf{n_3} &= (\mathbf{p_2} - \mathbf{p_1}) \times (\mathbf{p_3} - \mathbf{p_1}) \\
\mathbf{n_2} &= \mathbf{n_3} \times (\mathbf{p_5} - \mathbf{p_4}) \\
\mathbf{n_1} &= \mathbf{n_2} \times \mathbf{n_3} \\
D_3 &= \mathbf{p_2} \cdot \mathbf{n_1} \\
D_2 &= \mathbf{p_4} \cdot \mathbf{n_2} \\
D_1 &= \mathbf{p_6} \cdot \mathbf{n_3}
\end{aligned} \tag{B.1}$$

Where p_{1-6} are the measurement points as shown in figure B.4. The position of the original location of the intersection point of these planes with respect to the optical centre is known when the optical mount is

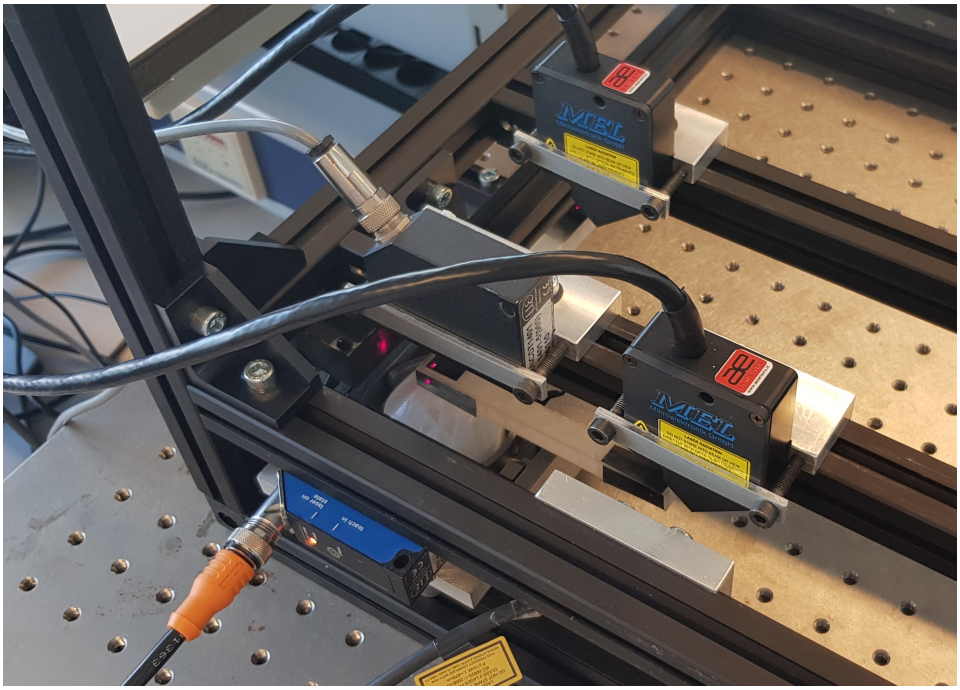

Figure B.3: A picture of the used measurement setup

in its initial state. An adjustment results in a displacement of this intersection point, the new position of the intersection point can be calculated using Cramer's rule:

$$\mathbf{I} = \frac{D_1(\mathbf{n_2} \cdot \mathbf{n_3}) + D_2(\mathbf{n_3} \cdot \mathbf{n_1}) + D_3(\mathbf{n_1} \times \mathbf{n_2})}{\mathbf{n_1} \bullet (\mathbf{n_2} \cdot \mathbf{n_3})} \tag{B.2}$$

The normal vectors $\mathbf{n_{1-3}}$ can also be used to define a rotation matrix R as shown in equation B.3.

$$R = [\mathbf{n_1 n_2 n_3}] \tag{B.3}$$

Displacement of intersection point I is caused by both translation and rotation of the optical mount. The translation can be found by subtracting the rotated vector $R \cdot I_0$ from the actual vector between O and I as shown in figure B.5. The rotations are calculated using the following equations.

$$\begin{aligned} R_x &= \arccos\left(\frac{\mathbf{n_3} \cdot \mathbf{e_3}}{|\mathbf{n_3} \cdot (\mathbf{e_2} + \mathbf{e_3})|}\right) \\ R_y &= \arccos\left(\frac{\mathbf{n_3} \cdot \mathbf{e_3}}{|\mathbf{n_3} \cdot (\mathbf{e_1} + \mathbf{e_3})|}\right) \\ R_z &= \arccos\left(\frac{\mathbf{n_2} \cdot \mathbf{e_2}}{|\mathbf{n_2} \cdot (\mathbf{e_1} + \mathbf{e_2})|}\right) \end{aligned} \tag{B.4}$$

Where $R_{x,y,z}$ are the rotations around the X, Y and Z axis. $\mathbf{e_{1-3}}$ are the unit vectors of the reference coordinate system which is shown in figure B.6.

B.3. Results

The graphs in figures B.7, B.8, B.9 and B.10 show the resulting crosstalk in prototype 3 as a result of the adjustable DOFs.

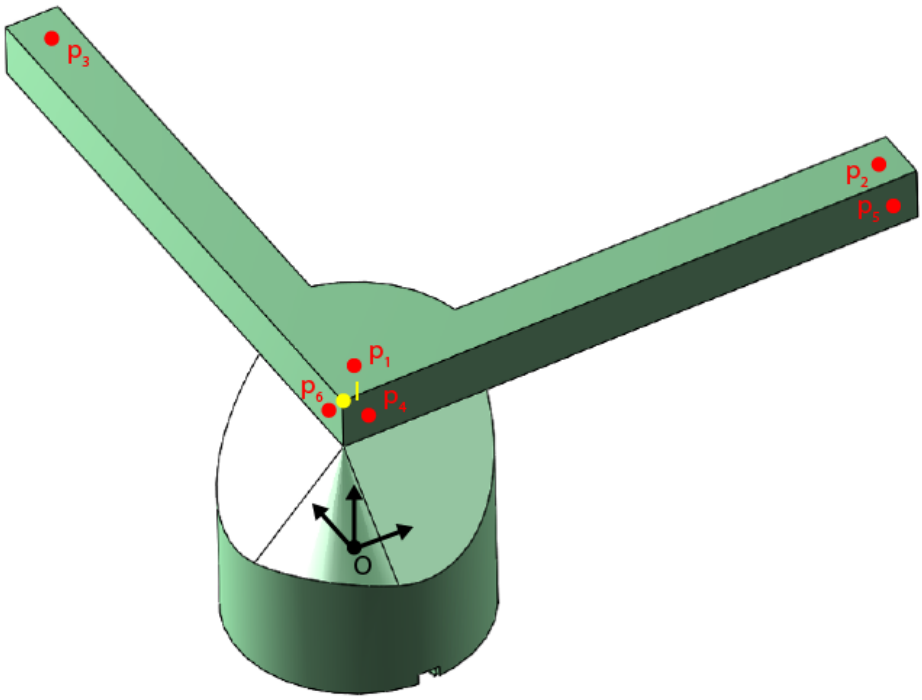

Figure B.4: The measurement tool with the measured points p_{1-6}, the initial coordinate system O and the intersection point of the planes I as defined by p_{1-6}.

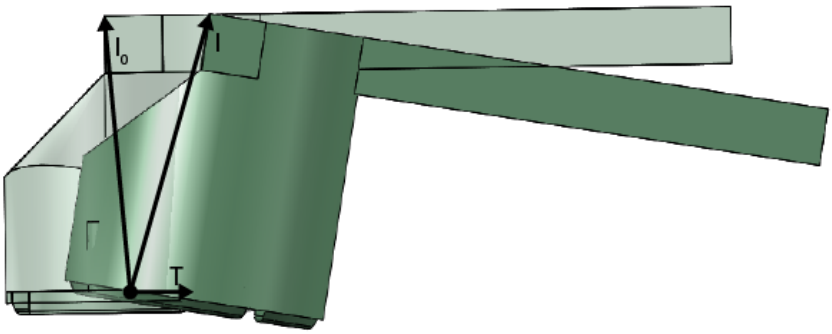

Figure B.5: Visualization of the calculation of the translation by subtracting the purely rotated intersection point from the actual intersection point

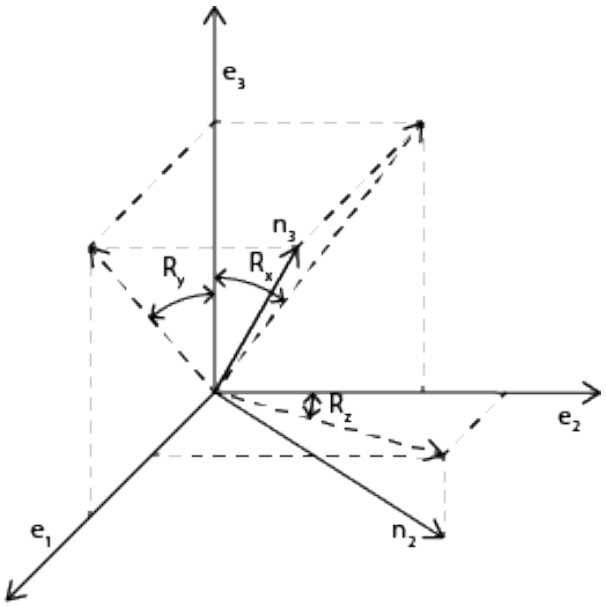

Figure B.6: Visualization of the calculation of the rotations where the angles are defined by the angle of the projected vector on the plane with the original vectors.

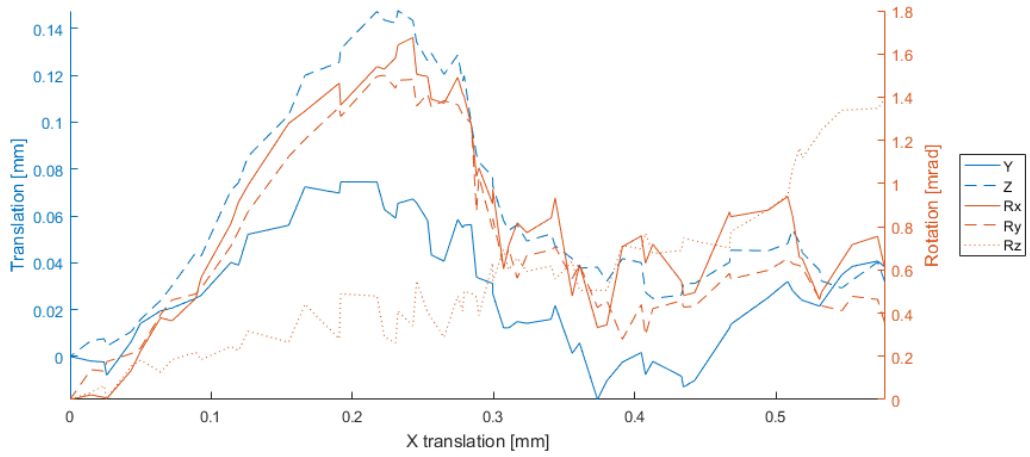

Figure B.7: Crosstalk as a result of X translation

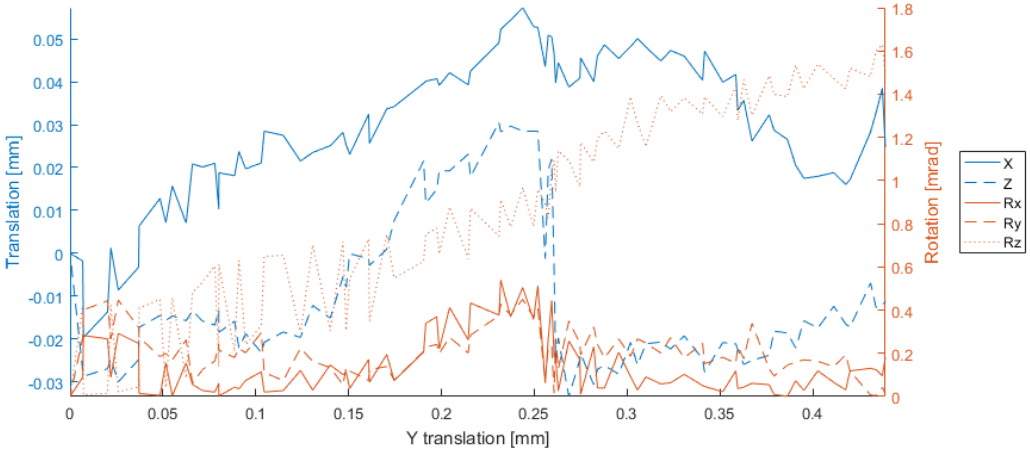

Figure B.8: Crosstalk as a result of Y translation

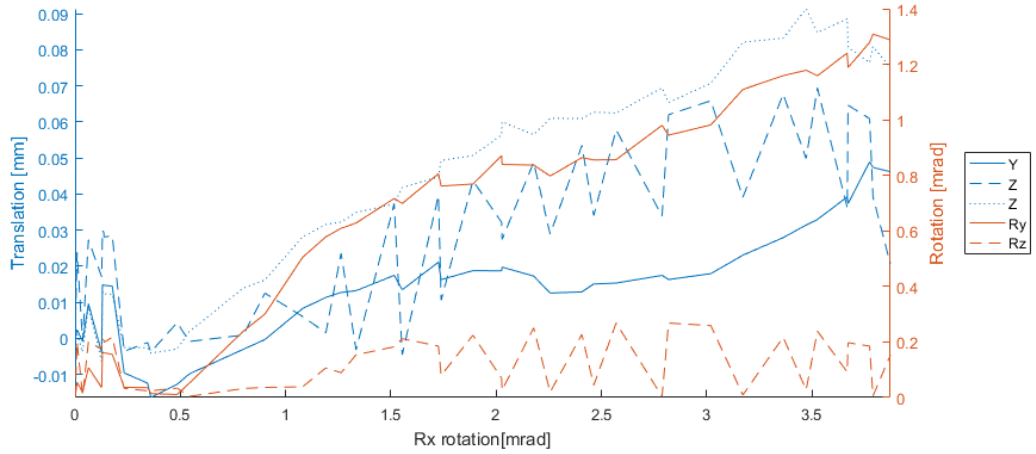

Figure B.9: Crosstalk as a result of rotation around the X-axis

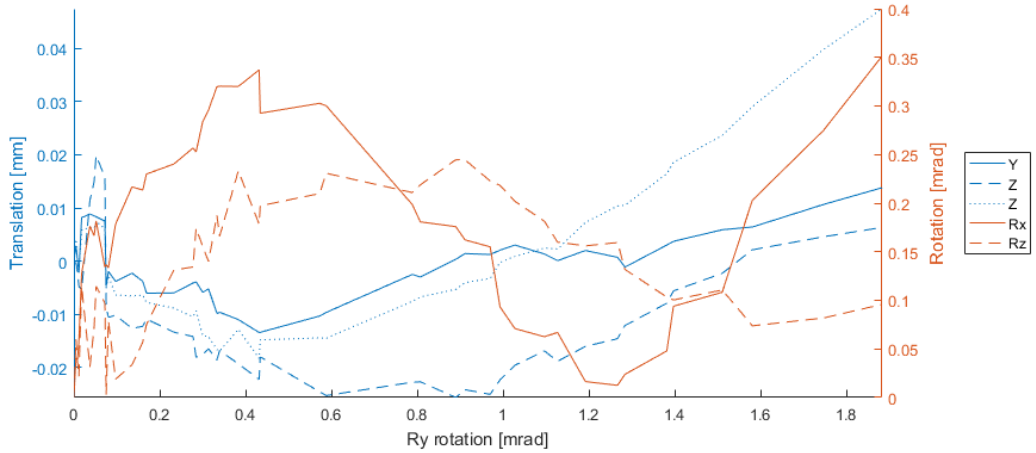

Figure B.10: Crosstalk as a result of rotation around the X-axis

Bibliography

[1] Shorya Awtar and Alexander H Slocum. Constraint-based design of parallel kinematic xy flexure mechanisms. *Journal of Mechanical Design*, 129(8):816–830, 2007.

[2] Shorya Awtar, John Ustick, and Shiladitya Sen. An xyz parallel-kinematic flexure mechanism with geometrically decoupled degrees of freedom. *Journal of Mechanisms and Robotics*, 5(1):015001–015001, 2012. ISSN 1942-4302. 10.1115/1.4007768.

[3] Umesh Bhagat, Bijan Shirinzadeh, Leon Clark, Peter Chea, Yanding Qin, Yanling Tian, and Dawei Zhang. Design and analysis of a novel flexure-based 3-dof mechanism. *Mechanism and Machine Theory*, 74: 173–187, 2014.

[4] Kee-Bong Choi and Doo-Hyeong Kim. Monolithic parallel linear compliant mechanism for two axes ultraprecision linear motion. *Review of scientific instruments*, 77(6):065106, 2006.

[5] Martin L Culpepper and Gordon Anderson. Design of a low-cost nano-manipulator which utilizes a monolithic, spatial compliant mechanism. *Precision engineering*, 28(4):469–482, 2004.

[6] Bingxiao Ding and Yangmin Li. Design and analysis of a decoupled xy micro compliant parallel manipulator. In *Robotics and Biomimetics (ROBIO), 2014 IEEE International Conference on*, pages 1898–1903. IEEE, 2014.

[7] Zhang Fan and Liu Yan. Type synthesis of a fully decoupled parallel wrist manipulator. In *Measuring Technology and Mechatronics Automation (ICMTMA), 2011 Third International Conference on*, volume 3, pages 1068–1071. IEEE, 2011.

[8] I. Gibson, D. Rosen, and B. Stucker. *Additive manufacturing technologies: 3D printing, rapid prototyping, and direct digital manufacturing, second edition.* 2015. doi: 10.1007/978-1-4939-2113-3. cited By 198.

[9] Z Guo, Y Tian, C Liu, F Wang, X Liu, B Shirinzadeh, and D Zhang. Design and control methodology of a 3-dof flexure-based mechanism for micro/nano-positioning. *Robotics and Computer-Integrated Manufacturing*, 32:93–105, 2015.

[10] G. Hao. Towards the design of monolithic decoupled xyz compliant parallel mechanisms for multi-function applications. *Mechanical Sciences*, 4(2):291–302, 2013. ISSN 21919151 (ISSN). Cited By :12 Export Date: 12 October 2016 Correspondence Address: Hao, G.; Department of Electrical and Electronic Engineering, School of Engineering, University College Cork, Cork, Ireland; email: g.hao@ucc.ie.

[11] Guangbo Hao. A 2-legged xy parallel flexure motion stage with minimised parasitic rotation. *Proceedings of the Institution of Mechanical Engineers, Part C: Journal of Mechanical Engineering Science*, 228(17): 3156–3169, 2014.

[12] Guangbo Hao and Xianwen Kong. A 3-dof translational compliant parallel manipulator based on flexure motion. In *ASME 2009 International Design Engineering Technical Conferences and Computers and Information in Engineering Conference*, pages 101–110. American Society of Mechanical Engineers, 2009.

[13] Guangbo Hao and Xianwen Kong. Novel xy compliant parallel manipulators for large displacement translation with enhanced stiffness. In *ASME 2010 International Design Engineering Technical Conferences and Computers and Information in Engineering Conference*, pages 1037–1047. American Society of Mechanical Engineers, 2010.

[14] Guangbo Hao and Xianwen Kong. Design and modeling of a large-range modular xyz compliant parallel manipulator using identical spatial modules. *Journal of Mechanisms and Robotics*, 4(2):021009, 2012. ISSN 1942-4302.

[15] Guangbo Hao and Haiyang Li. Conceptual designs of multi-degree of freedom compliant parallel manipulators composed of wire-beam based compliant mechanisms. *Proceedings of the Institution of Mechanical Engineers, Part C: Journal of Mechanical Engineering Science*, 229(3):538–555, 2015.

[16] Guangbo Hao and Haiyang Li. Design of 3-legged xyz compliant parallel manipulators with minimised parasitic rotations. *Robotica*, 33(4):787–806, 2015.

[17] Guangbo Hao and Jingjun Yu. Design, modelling and analysis of a completely-decoupled xy compliant parallel manipulator. *Mechanism and Machine Theory*, 102:179–195, 2016.

[18] Eric R Homer, Matthew B Harris, Shannon A Zirbel, Joanna A Kolodziejska, Henry Kozachkov, Brian P Trease, John-Paul C Borgonia, Gregory S Agnes, Larry L Howell, and Douglas C Hofmann. New methods for developing and manufacturing compliant mechanisms utilizing bulk metallic glass. *Advanced Engineering Materials*, 16(7):850–856, 2014.

[19] Larry L Howell. *Compliant mechanisms*. John Wiley & Sons, 2001.

[20] Larry L Howell, Spencer P Magleby, and Brian M Olsen. *Handbook of compliant mechanisms*. John Wiley & Sons, 2013.

[21] Jiming Huang, Yangmin Li, and Xinhua Zhao. Optimization of a completely decoupled flexure-based parallel xy micro-motion stage. In *Mechatronics and Automation (ICMA), 2011 International Conference on*, pages 69–74. IEEE, 2011.

[22] S Kota, K-J Lu, Z Kreiner, B Trease, J Arenas, and J Geiger. Design and application of compliant mechanisms for surgical tools. *Journal of biomechanical engineering*, 127(6):981–989, 2005.

[23] Sridhar Kota, Jinyong Joo, Zhe Li, Steven M Rodgers, and Jeff Sniegowski. Design of compliant mechanisms: applications to mems. *Analog integrated circuits and signal processing*, 29(1-2):7–15, 2001.

[24] H. Li, G. Hao, and R. C. Kavanagh. A new xyz compliant parallel mechanism for micro-/nano-manipulation: Design and analysis. *Micromachines*, 7(2), 2016. Export Date: 14 December 2016.

[25] Haiyang Li, Guangbo Hao, and Richard Kavanagh. Synthesis of decoupled spatial translational compliant parallel mechanisms via freedom and actuation method (fam). In *ASME 2014 12th Biennial Conference on Engineering Systems Design and Analysis*, pages V003T17A004–V003T17A004. American Society of Mechanical Engineers, 2014.

[26] Haiyang Li, Guangbo Hao, and Richard C Kavanagh. A new xyz compliant parallel mechanism for micro-/nano-manipulation: Design and analysis. *Micromachines*, 7(2):23, 2016.

[27] Yangmin Li and Qingsong Xu. Design and optimization of an xyz parallel micromanipulator with flexure hinges. *Journal of Intelligent and Robotic Systems*, 55(4-5):377, 2009. ISSN 0921-0296.

[28] Yangmin Li and Qingsong Xu. A totally decoupled piezo-driven xyz flexure parallel micropositioning stage for micro/nanomanipulation. *IEEE Transactions on Automation Science and Engineering*, 8(2): 265–279, 2011. ISSN 1545-5955.

[29] Yangmin Li, Jiming Huang, and Hui Tang. A compliant parallel xy micromotion stage with complete kinematic decoupling. *IEEE Transactions on Automation Science and Engineering*, 9(3):538–553, 2012.

[30] Xin-Jun Liu, Jinsong Wang, Feng Gao, and Li-Ping Wang. On the design of 6-dof parallel micro-motion manipulators. In *Intelligent Robots and Systems, 2001. Proceedings. 2001 IEEE/RSJ International Conference on*, volume 1, pages 343–348. IEEE, 2001.

[31] Tien-Fu Lu, Daniel C Handley, Yuen Kuan Yong, and Craig Eales. A three-dof compliant micromotion stage with flexure hinges. *Industrial Robot: An International Journal*, 31(4):355–361, 2004.

[32] John E McInroy and Jerry C Hamann. Design and control of flexure jointed hexapods. *IEEE Transactions on Robotics and Automation*, 16(4):372–381, 2000.

[33] Huy-Hoang Pham, I-Ming Chen, and Hsien-Chi Yeh. Micro-motion selective-actuation xyz flexure parallel mechanism: design and modeling. 2003.

[34] Singiresu S Rao and Fook Fah Yap. *Mechanical vibrations*, volume 4. Prentice Hall Upper Saddle River, 2011.

[35] Stuart T Smith. *Flexures: elements of elastic mechanisms*. CRC Press, 2014.

[36] Herman Soemers. *Design Principles for precision mechanisms*. T-Pointprint, 2011.

[37] Doug Stewart. A platform with six degrees of freedom. *Proceedings of the institution of mechanical engineers*, 180(1):371–386, 1965.

[38] Xiantao Sun, Weihai Chen, Rui Zhou, Wenjie Chen, and Jianbin Zhang. A decoupled 2-dof flexure-based micropositioning stage with large travel ranges. *Robotica*, 32(5):677–694, 2014.

[39] Xueyan Tang, I-Ming Chen, and Qing Li. Design and nonlinear modeling of a large-displacement xyz flexure parallel mechanism with decoupled kinematic structure. *Review of Scientific Instruments*, 77 (11):115101, 2006.

[40] Qingsong Xu. Design and development of a compact flexure-based xy precision positioning system with centimeter range. *IEEE Transactions on Industrial Electronics*, 61(2):893–903, 2014.

[41] Qingsong Xu and Yangmin Li. Design of a partially decoupled high precision xyz compliant parallel micromanipulator. In *Nano/Micro Engineered and Molecular Systems, 2008. NEMS 2008. 3rd IEEE International Conference on*, pages 13–18. IEEE, 2008. ISBN 1424419077.

[42] Li Yang, Keng Hsu, Brian Baughman, Donald Godfrey, Francisco Medina, Mamballykalathil Menon, and Soeren Wiener. *Additive Manufacturing of Metals: The Technology, Materials, Design and Production*. Springer, 2017.

[43] Jingjun Yu, Yan Xie, Zhenguo Li, and Guangbo Hao. Design and experimental testing of an improved large-range decoupled xy compliant parallel micromanipulator. *Journal of Mechanisms and Robotics*, 7 (4):044503, 2015.

[44] Yi Yue, Feng Gao, Xianchao Zhao, and Q Jeffrey Ge. Relationship among input-force, payload, stiffness, and displacement of a 6-dof perpendicular parallel micromanipulator. *Journal of Mechanisms and Robotics*, 2(1):011007, 2010.

[45] Yuan Yun and Yangmin Li. Design and analysis of a novel 6-dof redundant actuated parallel robot with compliant hinges for high precision positioning. *Nonlinear Dynamics*, 61(4):829–845, 2010.

[46] Zhen Zhang, Binbin Liu, Peng Wang, and Peng Yan. Design of an additive manufactured xy compliant manipulator with spatial redundant constraints. In *Control Conference (CCC), 2016 35th Chinese*, pages 9149–9154. IEEE, 2016.